A novel Notch and WNT signaling mechanism contribute to pediatric DCM: a pathway to new therapeutics.

Obed O. Nyarko, MD[1, 2], Ethan Rausch, BS[2], Jared R.H. Goff, BS[3], Anis Karimpour-Fard, PhD[4], Caitlyn S. Conard, BS[2], Laura Hernandez-Lagunas, MS[2], Mckenna P.A. Burns, PhD[2], Brisa Peña, PhD[2,5], Shelley D. Miyamoto, MD[6#], Brian L. Stauffer, MD[2#], Carmen C. Sucharov, PhD[2#].

[1]Integrative Physiology Graduate Program, University of Colorado Anschutz Medical Campus, Aurora, CO 80045, USA.

[2]Department of Medicine, Division of Cardiology, University of Colorado Anschutz Medical Campus, Aurora, CO 80045, USA.

[3]University of Utah Department of Internal Medicine.

[4]Department of Medicine, Division of General Internal Medicine, University of Colorado School of Medicine, Aurora, CO, 80045.

[5]Bioengineering Department, University of Colorado Denver Anschutz Medical Campus, Aurora, Colorado, 80045.

[6]Department of Pediatrics, Division of Cardiology, University of Colorado Anschutz Medical Campus, Aurora, CO 80045, USA.

Short title: Novel mechanism of DCM via Notch and WNT.

[#]Corresponding authors:

Carmen C. Sucharov. 12700 E. 19th Ave., B-139 Aurora, Aurora, CO 80045, USA. kika.sucharov@cuanschutz.edu

Brian Stauffer. 12700 E. 19th Ave., B-139 Aurora, Aurora, CO 80045, USA. brian.stauffer@cuanschutz.edu

Shelley Miyamoto. 12700 E. 19th Ave., B-139 Aurora, Aurora, CO 80045, USA.
Shelley.miyamoto@childrenscolorado.org

Total word count: 9,081

ABSTRACT

Background

Idiopathic dilated cardiomyopathy (iDCM) in children is a life-threatening disease. Little is known about its cellular and transcriptional landscape, and the lack of disease-specific animal models limits our understanding of its mechanisms. We previously demonstrated that pediatric iDCM serum-circulating proteins promote pathologic remodeling *in vitro*, and that secreted frizzled related protein 1 (sFRP1) increases stiffness in cardiomyocytes. Here we investigated the mechanisms by which sFRP1 contributes to cardiac dysfunction.

Methods

The effect of sFRP1 in combination with isoproterenol (ISO) (to recapitulate the increase in circulating catecholamine observed in pediatric DCM patients) was evaluated in neonatal rat ventricular myocytes (*in vitro*), and in neonatal rats through intraperitoneal injections (*in vivo*). Function and molecular mechanisms were investigated through echocardiography and next-generation-sequencing respectively. Protein levels and localization were determined by Western blot. Tissue stiffness was measured by Atomic Force Microscopy. *In vitro* and *in vivo* data were compared to explanted human heart tissue (*ex vivo*).

Results

We show that ISO+sFRP1 reactivates the fetal gene program *in vitro,* and promotes cardiac dysfunction, dilation and stiffness *in vivo*. Importantly, we show stiffness is also increased in pediatric iDCM hearts. We identified co-activation of Notch and WNT signaling in both ISO+sFRP1-treated rats and pediatric iDCM hearts. Mechanistically, *in*

vitro inhibition of Notch or β-catenin prevented pathological remodeling, and Notch inhibition improved cardiac function and reduced ventricular dilation in ISO+sFRP1-treated rats and NRVMs.

Conclusion

We identified concordant alterations in Notch and WNT signaling in pediatric iDCM hearts and in our ISO+sFRP1-treated rats. Notch inhibition abrogated pathologic changes *in vitro* and *in vivo*. These findings provide novel mechanistic insights and a potential therapeutic target for pediatric iDCM.

Keywords- Pediatric, Heart failure, dilated cardiomyopathy, stiffness, Notch, WNT,

Clinical perspective

What is new?

- iDCM in children continues to be poorly understood due to the lack of an animal model and lack of understanding of the disease mechanisms.
- This study establishes a unique young rat model that recapitulates key features of the disease, which include impaired systolic function with ventricular dilation, myocardial stiffness and distinct transcriptomic signatures.
- This study investigates molecular pathways commonly altered in pediatric iDCM heart and our novel animal model.

What are the clinical implications

- We identified Notch and WNT co-activation as key regulators of pathological remodeling and cardiac dysfunction, and show that inhibition of Notch signaling

can prevent pathological remodeling and cardiac dysfunction, suggesting targeting the Notch pathway may be a viable option to treat pediatric DCM.

- These findings provide a preclinical model to investigate targeted interventions for pediatric DCM.

INTRODUCTION

Idiopathic dilated cardiomyopathy (iDCM) is one of the main causes of cardiac-related mortality in children. Pediatric iDCM is a rare disease, making it very difficult to perform large, randomized placebo-controlled clinical trials (RCTs) in this population. The first RCT performed in children with heart failure (HF) studied the non-selective β-adrenergic receptor (β–AR) blocker, carvedilol. Importantly, although carvedilol has been shown to decrease morbidity and mortality in adults with DCM, the results of the trial were neutral in children[1], even though there are similarities in the pathophysiology of HF in children and adults, including increased circulating catecholamines[2,3]. Unfortunately, to date, there is limited evidence to support the treatment of HF in children, and current therapies are largely based on extrapolation of guideline-directed medical therapy (GDMT) for adult patients without proven efficacy in children.

Existing animal models of HF in children tend to focus on specific genetic mutations. However, only about one-third of children with iDCM have any identified pathogenic genetic variant[4], making use of any single genetic model difficult to generalize to the pediatric iDCM population. The lack of a generalizable animal model has negatively impacted the ability to investigate mechanisms of disease and identify targeted therapeutic options, which likely contributes to the fact that pediatric HF outcomes lag behind those of adults[5]. There is, however, a growing appreciation that molecular and cellular pathologic remodeling in pediatric HF is unique and lacks the well-known phenotypic changes observed in the adult heart[6]. We and others have shown that pediatric iDCM hearts have minimal fibrosis[5,7], lack cardiomyocyte hypertrophy[5,8], display

133 an age-specific transcriptome profile[5,8], unique changes to the β–AR system[9], and
134 diminished immune cell response[5].
135
136 In the pathological state, the heart responds by reverting to the fetal gene program
137 (FGP)[10], which includes re-expression of natriuretic peptides (*NPPA*/*NPPB*) and reduced
138 expression of the ratio α/β-Myosin Heavy Chain (MHC–*Myh6/Myh7*)[10,11]. We tested the
139 effect of the pediatric iDCM secretome on gene expression and cellular stiffness in
140 primary cardiomyocytes and showed that circulating proteins contribute to pathologic
141 changes in cells[12]. We further showed that the protein secreted frizzled protein 1 (sFRP1)
142 is increased in the serum and hearts of patients with iDCM and promoted cellular stiffness
143 in primary cardiomyocytes[12]. sFRP1 is known to modulate the WNT signaling pathway[13].
144 WNT ligands regulate cellular activities through the activation of β-catenin-dependent
145 (canonical) and independent (non-canonical) pathways[13]. The WNT signaling pathway
146 influences Notch signaling activity in various cellular and developmental contexts. In
147 cardiogenesis, both WNT and Notch signaling pathways are crucial in determining cell
148 fate and survival[14,15]. The activity of Notch signaling is usually reduced in the postnatal
149 heart but increased in cases of damage or injury[16]. Activation of the Notch receptors and
150 subsequent cleavage by ADAM metalloproteinases and γ-secretase leads to the release
151 of the Notch intracellular domain (NICD) in the cytoplasm, which translocates to the
152 nucleus and activates transcription of Notch target genes resulting in cell specific
153 effects[14].
154

155 In this study we investigated the effect of sFRP1 *in vitro* and *in vivo* through the
156 development of a novel animal model that consists of intraperitoneal injections of sFRP1
157 and isoproterenol (to recapitulate the increase in circulating catecholamine observed in
158 pediatric DCM patients)[2,3]. We show that this model reproduces aspects of pediatric
159 iDCM, including decreased cardiac function associated with dilation, and activation of
160 Notch and WNT signaling. We further show that ISO+sFRP1 promotes cardiac stiffness,
161 and importantly, inhibiting Notch signaling prevents pathological remodeling and cardiac
162 dysfunction.

163

164 **RESULTS**

165 **Human Samples**

166 Detailed demographics from all patients included in the study are depicted in
167 Supplemental Table 1. Median age for DCM patients was 3.9 years (interquartile range-
168 IQR=6.2), with an average EF of 17.33%, 58.3% were female, 8.3% were on beta-
169 blockers, all were on angiotensin converting enzyme inhibitors (ACEi) and 75% were on
170 a phosphodiesterase 3-inhibitor (PDE3i). Non-failing control (NF) subject had a median
171 age of 6.9 years (IQR=9.5), 28.6% were female and 14.3% were on beta-blockers.

172

173 **sFRP1 and ISO treatment promotes pathological remodeling *in vitro***

174 We first evaluated if treatment with ISO and/or sFRP1 promoted pathological remodeling
175 i*n vitro*. NRVMs were treated with ISO, sFRP1 or a combination of both factors for 72
176 hours. Fetal gene program (FGP), as measured by upregulation of *NPPA, NPPB*, and a
177 decrease in the ratio of α-myosin heavy chain (*MYH6*) to β-myosin heavy chain (*MYH7*),
178 was observed only when cells were treated with ISO+sFRP1. *NPPA* increased in both
179 sFRP1 ($p=0.0379$) and ISO+sFRP1-treated cells ($p<0.0001$), *NPPB* increased in ISO
180 ($p<0.0001$) and ISO+sFRP1-treated cells ($p<0.0001$), while *MYH6/MYH7* decreased in
181 response to sFRP1 ($p<0.0001$) and ISO+sFRP1 treatments ($p=0.0142$) (**Fig.** 1a). sFRP1
182 expression increased in cells treated with ISO+sFRP1 ($p=0.0111$) (**Fig.** 1b). Furthermore,
183 the increase in sFRP1 gene expression in ISO+sFRP1-treated cells positively correlated
184 with *NPPA* ($p=0.0004$) and *NPPB* expression ($p<0.0001$) and negatively correlated with
185 *MYH6/MYH7* ($p<0.0001$) (Supp. **Fig.** 1). These results suggest that a combination of ISO
186 and sFRP1 promote pathological remodeling *in vitro*.

187

188 **sFRP1 and ISO treatment promotes cardiac dysfunction and dilation in a young**
189 **rodent model**

190 To further validate the translational relevance of the *in vitro* model, we tested the effect of
191 ISO+sFRP1 *in vivo*. Rats were injected with ISO and/or sFRP1 intraperitoneally for 2
192 weeks (**Fig.** 1c). Rats injected with ISO+sFRP1 had significantly reduced ejection fraction
193 (EF) ($p<0.0001$) when compared to vehicle-treated control rats, as well as when
194 compared to rats injected solely with ISO ($p=0.0316$) or sFRP1 ($p<0.0001$) (**Fig.** 1d).
195 Echocardiogram findings also showed that left ventricular volume in systole (LV vol(s))
196 increased in ISO+sFRP1-treated rats compared to vehicle-treated controls ($p=0.0002$),
197 ISO-treated rats ($p=0.0306$) or sFRP1-treated rats ($p=0.0006$) (**Fig.** 1e). Similarly, left
198 ventricular internal diameter in systole (LVID(s)) increased in ISO+sFRP1 rats compared
199 to vehicle-treated controls ($p<0.0001$), ISO-treated rats ($p=0.0334$) or sFRP1-treated rats
200 ($p<0.0001$) (**Fig.** 1f). There were no significant differences in left ventricular anterior and
201 posterior wall thickness for any of the treated groups (**Fig.** 1g, h). Diastolic parameters,
202 LV vol(d) and LVID(d), followed the same trend as systolic parameters (Supp Fig. 2a, b).
203 Morphometric data showed a significant increase in whole heart to body weight and LV
204 weight to body weight ratios in ISO+sFRP1 rats compared to vehicle-treated controls
205 (Supp. Fig. 2c, d). Functional alterations were not restricted to male animals; changes
206 were also observed in females (Supp Fig. 2e).

207

208 As in the *in vitro* expression studies, *NPPA* expression increased in sFRP1- (p=004) and
209 ISO+sFRP1-treated rats ($p=0.0035$) compared to vehicle-treated controls (Supp. Fig 3a).
210 However, *NPPB* expression only increased in sFRP1-treated rats ($p=0.0011$) and not in

211 response to ISO+sFRP1 treatment (Supp. Fig 3b). *MYH6/MYH7* ratio decreased in both
212 sFRP1 (p=0.0272) and ISO+sFRP1 rats (p=0.049) (Supp. Fig 3c). A simple linear
213 regression was performed to evaluate the relationship between pathological cardiac
214 remodeling, evidenced by reactivation of the FGP, and ejection fraction. We found that
215 the relative expression of *NPPA*, but not *NPPB*, was significantly correlated with a
216 decrease in EF (p=0.0039) (Supp. Fig 4a), whereas the ratio of *MYH6/MYH7* trended
217 towards a positive correlation (higher *MYH6/MYH7* correlated with higher EF) (p=0.0825)
218 (Supp. Fig 4b). These results, together with the *in vitro* data, provide evidence that
219 ISO+sFRP1 promotes pathological remodeling *in vitro* and cardiac dysfunction
220 associated with left ventricular dilation *in vivo.*
221
222 To investigate the translational significance of the rat ISO+sFRP1 DCM model, we
223 investigated cardiac mRNA and serum sFRP1 levels in rats relative to our published data
224 in human pediatric DCM patients[8,12]. We observed a significant increase in cardiac sFRP1
225 mRNA levels in ISO+sFRP1 rats (p=0.0003) (**Fig.** 2a) that was negatively correlated with
226 EF (p=0.0121) (Supp. Fig 5a). Moreover, levels of sFRP1 in the serum of ISO+sFRP1
227 rats were significantly higher than vehicle-treated controls (**Fig.** 2b) (p=0.0146). There
228 was a trend to negative correlation when analyzing levels of serum circulating sFRP1 and
229 EF (p=0.0888) in rats (Supp. Fig 5b). The observed increase in rat cardiac and serum
230 sFRP1 levels was comparable to our previously published human data[12].
231
232 **ISO+sFRP1 promotes increased stiffness in the absence of myocyte hypertrophy**
233 **or fibrosis.**

234 We previously showed that DCM serum or sFRP1 treatment promotes stiffness in NRVMs
235 assessed by atomic force microscopy (AFM)[12]. To further explore if sFRP1 promotes
236 stiffness *in vivo*, we investigated myocardial stiffness in rats. As shown in **Fig.** 2c-e,
237 ISO+sFRP1 promoted a significant increase in LV stiffness when compared to vehicle-
238 treated control rats (p=0.02). Stiffness is specific to cardiac dysfunction as changes in
239 myocardial stiffness were not observed in rats treated with ISO only or sFRP1 only (Supp.
240 Fig. 6a-d). Importantly, we tested stiffness in the LV of children with DCM and show that
241 stiffness is increased when compared to NF healthy controls (p=0.0176) (**Fig.** 2f-h).
242
243 We and others previously showed that pediatric DCM patients have minimal fibrosis and
244 lack myocyte hypertrophy[5,17]. Compared to vehicle-treated controls, ISO+sFRP1 rats did
245 not exhibit increased fibrosis, as determined by Masson's trichrome staining (Supp. Fig.
246 7a-c). Additionally, RT-qPCR analysis of the rat LV tissue demonstrated no significant
247 upregulation of profibrotic genes, including *COL1A1, COL3A1, Galectin-3, TGFB1*,
248 *TGFB2* and *TIMP1-4* (Supp. Fig 7d-l). Furthermore, myocyte hypertrophy was not
249 observed in ISO+sFRP1 rats compared to controls (Supp. Fig.7m-o).
250
251 **Notch signaling is altered in ISO+sFRP1 rats and in pediatric DCM hearts.**
252 To better understand the pathophysiology of ISO+sFRP1-mediated DCM and identify the
253 mechanisms underlying the disease, we performed bulk RNA sequencing analysis of the
254 LV of rats treated with ISO and/or sFRP1 compared to vehicle-treated controls
255 (n=6/group) (**Fig.** 3a). Of the 14,350 genes identified, there were 286 differentially
256 expressed genes (DEGs) (p<0.05) in ISO+sFRP1 rats compared to vehicle-treated
257 controls (113 up-regulated and 173 down-regulated) (Supp. Table 2). Unsupervised

258 hierarchical clustering separated control and ISO+sFRP1 treatment groups based on the
259 gene expression profile. Unsupervised hierarchical cluster heatmaps of the top 50 DEGs
260 in ISO+sFRP1- (**Fig.** 3b), sFRP1- or ISO-treated rats (supp. Fig. 8a, b) compared to
261 vehicle-treated controls were generated and showed a clear separation between
262 individual groups and control. Pathways were analyzed using the identified significantly
263 upregulated or downregulated genes. Pathway analysis of upregulated genes highlighted
264 Notch signaling pathway as one of the main dysregulated pathways associated with
265 upregulated genes uniquely enriched in response to ISO+sFRP1 compared to controls
266 (**Fig.** 3c). WNT/β-catenin signaling was the 2nd top pathway for all dysregulated DEGs in
267 ISO+sFRP1 rats (**Fig.** 3d). Pathway analysis was also done for downregulated genes
268 (Supp. Fig. 8c), and for ISO- or sFRP1-treated rats. The WNT/β-catenin signaling
269 pathway was significantly dysregulated in sFRP1-treated rats while mitochondrial
270 organization pathways were dysregulated in ISO-treated rats (Supp. Fig. 8d-g)
271
272 Importantly, in our prior investigations of explanted pediatric DCM hearts, we identified
273 changes in gene expression that suggested alterations in the Notch and WNT pathways[8].
274 To investigate commonalities in hearts from children with DCM and our rat model, we
275 assessed similarities between DEGs from ISO+sFRP1 rats, pediatric DCM hearts, and
276 from our previously published data on pediatric DCM serum-treated NRVMs[12].
277 Transcriptomic analysis revealed a substantial overlap in DEGs in the LV tissue of
278 ISO+sFRP1-treated rats and human DCM hearts or serum-treated cells. Notably, 96% of
279 DEGs in the LV tissue of ISO+sFRP1-treated rats were also observed in the human DCM
280 heart (65% unique only to human LV DEGs, 31% shared between human LV and rat LV
281 DEGs with only 4% DEGs unique to rats) (**Fig.** 3e). Additionally, 57% of DEGs were

282 common between the LV tissue of ISO+sFRP1-treated rats and NRVMs treated with
283 human DCM serum (57% unique only to NRVMs treated with human DCM serum DEGs,
284 1% shared between NRVMs treated with human DCM serum DEGs and rat LV DEGs
285 with 42% DEGs unique to rats) (**Fig.** 3f). Again, Notch signaling was one of the top
286 dysregulated pathways associated with commonly upregulated genes in DCM serum-
287 treated NRVMs and LV tissue of ISO+sFRP1-treated rats (**Fig.** 3g).
288

289 **Single-nuclei RNA sequencing (snRNA-seq) identifies activation of Notch and β-**
290 **catenin signaling in response to ISO+sFPR1**

291 To further characterize the cell types and biological mechanisms altered at the individual
292 cellular level, we performed single-nuclei RNA sequencing of LV tissue from ISO and/or
293 sFRP1, and vehicle-treated control rats (n=3/group). A total of 9,214 nuclei in control,
294 11,588 nuclei in ISO-, 13,758 nuclei in sFRP1-, and 11,127 in ISO+sFRP1-treated rats
295 were identified after cells were pooled. Clusters were annotated based on canonical cell
296 marker expression (supp. Table 3). We assessed the distribution of cell-type annotated
297 nuclei across all samples and identified 26 transcriptionally distinct cell-type clusters
298 marked by canonical gene markers (**Fig.** 4a)[18,19]. The proportions of the different
299 identified cell types varied across treatment groups. Representation of the various cell
300 type distribution showed an increase in the relative ratio of ventricular cardiomyocytes in
301 the ISO+sFRP1-treated rats (**Fig.** 4b, c, supp. Table 3). A sub-analysis of ventricular
302 cardiomyocytes identified eight different sub-clusters (**Fig.** 4d). Pathway analysis of
303 dysregulated DEGs in the ISO+sFRP1 ventricular cardiomyocyte subcluster 2 (the cluster
304 with the most relative proportion of ventricular cardiomyocytes) suggests activation of
305 Notch signaling as one of the top dysregulated pathways (**Fig.** 4e), and *CTNNB1* (β-

306 catenin) as one of the top transcription factors predicted to control expression of
307 upregulated genes (**Fig.** 4f). Additionally, pathway analysis suggests extracellular matrix
308 (ECM) proteoglycan enrichment as the top dysregulated pathway in subcluster 6 (cluster
309 with the 2nd most relative proportion of ventricular cardiomyocytes), and *Notch1* as one of
310 the top transcription factors predicted to control expression of dysregulated genes (**Fig.**
311 4g, h). We then used ClinVar to evaluate how DEGs in the ventricular cardiomyocyte
312 cluster relate to human health, and identified DCM as the top phenotype, which further
313 validates our model (**Fig.** 4i).
314
315 **Levels of Notch change *in vivo*, *in vitro* and in human DCM hearts.**
316 To further explore Notch signaling dysregulation in DCM, we investigated levels of Notch-
317 target genes and Notch intracellular domain (NICD), the constitutively active form of
318 Notch1, in the different models. We found increased expression of Notch target genes,
319 which was associated with increased nuclear and cytoplasmic NICD. NICD protein was
320 increased in cytoplasmic (p=0.0013) and nuclear (p=0.0143) fractions of pediatric DCM
321 hearts (**Fig.** 5a-d), in cytoplasmic (p=0.0053) and nuclear fractions (p=0.0086) of
322 ISO+sFRP1 rat hearts (**Fig.** 5e-h), and in cytoplasmic (p=0.0371) and nuclear (p =0.0119)
323 fractions of ISO+sFRP1-treated NRVMs (**Fig.** 5i-l). In parallel, we also observed
324 increased expression of Notch-target genes; *Hey1*, was upregulated in pediatric DCM
325 hearts (1.55x, q=0.02 from RNA-seq data)[8]. *Notch1* (p=0.0398) and *HEY1* (p=0.0467)
326 were up-regulated in ISO+sFRP1 rat hearts (**Fig.** 5m). *Notch1* (p=0.0276) together with
327 the expression of Notch target genes *HEY1* (p=0.0006), *HEY2* (p=0.0124), *HES1*
328 (p=0.0361) and *HEYL* (p=0.0436) were increased in NRVMs treated with ISO+sFRP1
329 compared to vehicle-treated controls (**Fig.** 5n). There was no increase in expression of

330 other Notch receptor genes such as Notch2-4 (Supp. Fig. 9a-c). Expression of *Notch 1*
331 and Notch-target genes in ISO or sFRP1-treated NRVMs did not change (Supp. 10a-e).
332
333 **Levels of β-catenin change *in vivo*, *in vitro* and in human DCM hearts**
334 sFRP1 is known to modulate the β-catenin pathway in a context-dependent manner[20]. As
335 shown in **Fig.** 3d our transcriptomic data strongly suggested the activation of the β-catenin
336 pathway in ISO+sFRP1-treated rats, which is in agreement with our published explanted
337 pediatric DCM heart data[8]. We tested expression of β-catenin gene *(CTNNB1)* and β-
338 catenin protein levels in the cytoplasmic and nuclear fractions of explanted pediatric DCM
339 hearts, ISO+sFRP1 rat hearts and ISO+sFRP1-treated NRVMS (**Fig.** 6). We found higher
340 levels of β-catenin in the cytoplasmic (p=0.0013) and nuclear (p=0.0433) fractions in DCM
341 hearts (**Fig.** 6a-d), in the cytoplasmic (p=0.0099) and nuclear fractions (p-value=0.0191)
342 of ISO+sFRP1 rat hearts (**Fig 6.** e-h), and in the cytoplasmic (p=0.0101) and nuclear
343 fractions (p=0.0039) of ISO+sFRP1-treated NRVMs (**Fig 6.** i-l). Additionally, we also
344 observed an increase in expression of *CTNNB1* (p=0.0263) in ISO+sFRP1 rats (**Fig.** 6m)
345 and ISO+sFRP1-treated NRVMs (p=0.0460) (**Fig.** 6n). Similar to what we observed when
346 evaluating Notch signaling, the increase in *CTNNB1* levels was unique to ISO+sFRP1-
347 treated NRVMs and was not observed in response to ISO or sFRP1. (Supp. Fig. 10f)
348
349 **β-catenin contributes to Notch activation in ISO+sFRP1-treated cells**
350 Others have reported an interplay between Notch and β-catenin signaling[21,22]. We next
351 evaluated the contribution of β-catenin to Notch activation. siRNA-mediated down-
352 regulation of *CTNNB1* in ISO+sFRP1-treated cells prevented ISO+sFRP1-mediated

353 activation of Notch target gene expression by blunting expression of *HEY1* (p<0.0001),
354 *HEY2* (p=0.0026), *HES1* (p=0.0167) and *HEYL* (p=0.0401) (**Fig.** 7a). Additionally, siRNA
355 for *CTNNB1* also prevented activation of the FGP by ISO+sFRP1 by blunting the increase
356 in expression of *NPPA* (p=0.0063) and *NPPB* (p=0.0003), and by increasing the ratio of
357 *MYH6/MYH7* (p=0.0446) (**Fig.** 7b). siRNA for *CTNNB1* also reduced the cytoplasmic
358 (p=0.0041) (**Fig.** 7c, d) and nuclear (p=0.0063) (**Fig.** 7e, f) increase of NICD by
359 ISO+sFRP1. The effect of si-CTNNB1 on β-catenin levels is shown in **Fig**. 8 c, e.
360

361 **Notch antagonism prevented pathological remodeling *in vitro* and cardiac**
362 **dysfunction associated with dilation *in vivo***

363 We also tested the effect of DAPT, a γ-secretase inhibitor known for reducing the levels
364 of NICD, on β-catenin levels and activation of the FGP. DAPT, as expected, prevented or
365 decreased the activation of Notch target genes HEY*1* (p<0.0001), *HEY2* (p=0.0004),
366 *HES1* (p<0.0001) and *HEYL* (p<0.0001) by ISO+sFRP1 (**Fig.** 8a). We next tested
367 whether Notch inhibition affected activation of the FGP. As shown in **Fig.** 8b. DAPT
368 prevented the reactivation of FGP by ISO+sFRP1 by blunting the increased expression
369 of *NPPA* (P=0.025), and *NPPB* (P=0.0014), and by increasing the ratio of *MYH6/MYH7*
370 (p=0.007). Additionally, DAPT prevented ISO+sFRP1-mediated increase in cytoplasmic
371 (p=0.0487) (**Fig.** 8c, d) and nuclear (p=0.0385) (**Fig.** 8e, f) β-catenin. DAPT also
372 prevented the increase in *CTNNB1* gene expression by ISO+sFRP1 (p=0.008) (**Fig.** 8g).
373 These data support the premise that the co-activation of Notch and β-catenin promotes
374 pathological remodeling.
375

376 Lastly, we investigated the role of DAPT in preventing cardiac dysfunction associated with
377 ventricular dilation in our ISO+sFRP1 *in vivo* model. DAPT prevented the reduction of EF
378 by ISO+sFRP1 (p=0.0048) and trended towards inhibiting the increase in LV vol(s)
379 (p=0.088) and LVID(s) (p=0.0935) (**Fig.** 8h). These results suggest that Notch inhibition
380 improves cardiac function in our rat model.
381

382 **DISCUSSION**

383 Studies focused on the mechanisms of HF in children are lacking. The rarity of the
384 disease, associated with the difficulty in performing studies in a vulnerable population,
385 has limited the development of age-specific therapies for pediatric iDCM, which
386 contributes to a relatively high rate of mortality in this population[23]. Currently, there is no
387 well-established disease model that accurately recapitulates the pathophysiology of
388 pediatric iDCM. Importantly, pediatric and adult iDCM differ in several key aspects,
389 including minimal myocardial fibrosis and no cardiomyocyte hypertrophy. These
390 differences could be due to age-dependent mechanisms or to intrinsic differences in the
391 disease process and may explain the differential response to medical therapies[24]. An
392 optimal *in vivo* model should, therefore, mirror not only the echocardiographic and
393 histological features but also the mechanistic characteristics of pediatric DCM. Our
394 ISO+sFRP1 rat model fulfills these criteria, by exhibiting ventricular dilation, cardiac
395 dysfunction, myocardial stiffness with minimal fibrosis, and activation of Notch-WNT
396 signaling, closely paralleling the pediatric iDCM phenotype.
397

398 **sFRP1-mediated pathologic remodeling and cardiac dysfunction**

399 We have previously shown that circulating sFRP1 levels are elevated in pediatric DCM
400 sera[12]. Likewise, catecholamines are increased in the serum of pediatric HF patients[3]. In
401 this study we found that *in vivo* co-administration of ISO+sFRP1 in neonatal rats results
402 in lower EF and LV dilation, and reactivation of the FGP. These findings suggest that β-
403 adrenergic stimulation primes cardiomyocytes to revert to a fetal-like transcriptional state,
404 which is a hallmark of maladaptive cardiac remodeling and HF and drives structural and
405 functional cardiac dysfunction *in vivo*.
406
407 **sFRP1 regulation of WNT signaling**
408 sFRP1 is traditionally viewed as a WNT signaling antagonist, which reduces β-catenin
409 levels. Our results suggest that sFRP1, in the context of β-adrenergic stimulation, acts as
410 a WNT agonist rather than an antagonist as evidenced by the increased levels of β-
411 catenin in ISO+sFRP1-treated cells and rats. Importantly, the increase in β-catenin levels
412 was also observed in explanted pediatric DCM hearts. In support of our findings, other
413 models of cardiac disease (such as myocardial infarction, cardiac fibrosis and HF) have
414 highlighted the role of sFRP1 in activating WNT signaling in response to cardiac injury[25].
415
416 Classically, sFRP1 inhibition of WNT signaling occurs relatively rapidly. Within the first 1-
417 6 hours of treatment, sFRP1 inhibits WNT signaling by directly binding to WNT ligands or
418 to frizzled receptors[26]. However, prolonged exposure and/or increased concentration of
419 sFRP1 can promote β-catenin stabilization and WNT signaling activation[27]. Our results
420 agree with these findings, as initial exposure to ISO+sFRP1 did not increase β-catenin
421 levels (not shown), but persistent (72 hours) exposure increased levels of β-catenin in

422 cardiomyocytes. The mechanisms associated with sFRP1-mediated stabilization of β-
423 catenin are unclear; sFRP1 may directly form complexes with frizzled receptors, possibly
424 mimicking the effects of WNT ligands or displacing inhibitory interactions, thus activating
425 downstream signaling[28]. Furthermore, it has been proposed that the duration or levels of
426 exposure to sFRP1 may stabilize certain WNT ligands or alter receptor dynamics to
427 enhance β-catenin accumulation[27].
428
429 Our results also suggest a context-dependent function of sFRP1, in which sFRP1 may
430 differentially modulate WNT signaling under adrenergic stress. In cancer, chronic
431 adrenergic stress has been shown to promote sFRP1 secretion, enhancing tumor growth
432 through β-catenin activation[27]. Hence targeting sFRP1 has been explored as a potential
433 therapeutic target for patients with adenocarcinoma[29]. Our findings extend these
434 observations by demonstrating that simultaneous β-adrenergic stimulation and WNT
435 pathway modulation can synergistically trigger maladaptive gene expression patterns and
436 cardiac dysfunction, which may be unique to the pediatric population. In this context, ISO
437 appears to act as a modulator of the response to sFRP1 and may modify the cellular
438 context, allowing WNT signaling components to become activated despite the presence
439 of a known antagonist, perhaps through non-canonical or compensatory mechanisms.
440
441 **WNT signaling in cardiac pathological remodeling**
442 WNT signaling is an essential pathway implicated in cell-cell communication and plays a
443 role in cardiac development, function and disease from embryonic stages to adult life[30].
444 The WNT/β-catenin pathway has a biphasic role in cardiac development and
445 differentiation, promoting cardiac differentiation before gastrulation and inhibiting cardiac

446 development after gastrulation[20]. Additionally, although stabilizing β-catenin promotes
447 proliferation of mammalian cardiomyocytes[31], it is also required for stress-induced cardiac
448 hypertrophy[32]. Furthermore, it has been suggested that active WNT/β-catenin signaling a
449 week after cardiac injury is involved in cardiac healing[33]. In contrast, depletion of β-catenin
450 attenuates ischemic cardiac remodeling through increased differentiation of resident
451 cardiac progenitor cells[34]. These studies highlight the complexity of WNT/β-catenin
452 signaling in the heart. In our study, we show that WNT/β-catenin contributes to a
453 pathological phenotype, suggesting the activation of this pathway in post-natal hearts is
454 associated with maladaptive remodeling and cardiac dysfunction.

455

456 **Notch and β-catenin axis promote DCM phenotype in a young rodent model**

457 Using transcriptomic data from our animal model, our data on molecular alterations in
458 pediatric iDCM hearts and serum-treated NRVMs, we explored molecular pathways
459 commonly altered in all models[8,12]. Importantly, of the genes altered in ISO+sFRP1 rat
460 hearts, the vast majority also changed in pediatric iDCM hearts (**Fig.** 3e). Additionally,
461 pathway analysis of DEGs in ISO+sFRP1 rat hearts and in pediatric iDCM hearts[8]
462 highlight activation of Notch and WNT signaling. Recent evidence has suggested a
463 crosstalk between the WNT and Notch signaling pathways in cardiac development and
464 disease[35]. Notch signaling is fundamentally involved in cell-cell communication and has
465 been implicated in cardiac development, function and cardiac birth defects[36]. Notch target
466 genes contribute to cardiac development and disease[37], and aberrations in the Notch
467 signaling pathway are associated with congenital heart defects[38]. In addition, Notch
468 signaling is activated after cardiac injury[39], and promotes cardiac regeneration[40], and

469 cellular stiffness[41]. These suggest that Notch might be beneficial in regenerative,
470 compliant environments such as the developing heart, but potentially detrimental in stiff,
471 non-regenerative conditions such as the postnatal heart.
472
473 Prior studies have shown that both Notch and WNT pathways can stimulate proliferation
474 of immature cardiomyocytes[42] and promote cardiomyocyte survival[43]. Notch signaling has
475 been shown to maintain the cardiac gene network needed for cardiac chamber formation
476 through WNT signaling[44]. In the heart, both pathways are tightly regulated during
477 embryogenesis, where they coordinate cardiac progenitor specification and
478 morphogenesis[40]. However, in disease states, their reactivation often contributes to
479 maladaptive remodeling[45]. Previous studies have shown that WNT/β-catenin signaling
480 can enhance Notch pathway activation through direct transcriptional regulation of Notch
481 ligands[21,22] while Notch signaling has been reported to modulate β-catenin stability and
482 nuclear translocation[46]. This bidirectional crosstalk may underlie the robust transcriptional
483 and protein response we observed in our data. In summary, the relationship between
484 Notch and WNT signaling is complex, dynamic, context dependent and is still being
485 explored, but both pathways are known to play critical roles in cardiac development,
486 homeostasis, and disease progression.
487
488 **The interplay between catecholamine and Notch and WNT signaling**
489 Interestingly, in our model, we observed an expansion of cardiomyocyte cluster 2 in
490 ISO+sFRP1 hearts. In this cluster, there is an upregulation of Notch signaling, and
491 *CTNNB1* is predicted to be one of the top transcriptional regulators, supporting our
492 findings that ISO+sFRP1 treatment results in WNT/Notch activation. Thus, the expansion

493 of ventricular cardiomyocyte nuclei in cluster 2 may reflect both a compensatory survival
494 mechanism and a shift toward a transcriptionally dysregulated state driven by concordant
495 Notch-WNT pathway synergy. In congruence, ventricular cardiomyocyte cluster 6
496 predicts *Notch1* as one of the top transcription factors predicted to control expression of
497 upregulated genes. This suggests that one cluster may be more β-catenin-regulated and
498 the other Notch-regulated.

499

500 In our model, we observe Notch signaling activation specifically in ISO+sFRP1-treated
501 NRVMs, but not when cells are treated with sFRP1 or ISO independently. This supports
502 the published data that chronic catecholamine stress may positively upregulate Notch
503 signaling via ADAM17-mediated catalytic cleavage, thereby linking the sympathetic
504 stress typical of HF to maladaptive developmental reprogramming[47].

505

506 Overall, these results suggest that catecholamines act not only as a stressor but also as
507 a molecular modulator, driving how cardiomyocytes convert developmental signals such
508 as WNT and Notch to pathological states that promote iDCM. To suggest a potential
509 crosstalk or relationship between the two pathways in the setting of ISO treatment, we
510 investigated the relationship between Notch and WNT signaling in our model. Down-
511 regulation of β-catenin in ISO+sFPR1-treated cells blunted the effect of Notch activation
512 on NICD protein levels and Notch target gene expression, and chemical inhibition of
513 Notch by DAPT blunted the increase of β-catenin by ISO+sFRP1. Our observation that
514 both pathways are upregulated in ISO+sFRP1-treated cells, rats, and human DCM hearts
515 suggests a cooperative role in driving pathological gene expression programs associated

516 with cardiac dysfunction and ventricular dilation *in vivo*. These findings support a model
517 in which combined β-adrenergic stimulation and increased WNT signaling activate
518 Notch–WNT signaling, contributing to sustained pathological remodeling and cardiac
519 dysfunction.

520

521 **Notch as a potential therapeutic target in pediatric iDCM.**

522 We also show that inhibiting Notch/WNT signaling prevents pathological remodeling.
523 Modulating these pathways could offer age-specific strategies for pediatric HF that differ
524 from adult therapies, especially in diseases like DCM. DAPT, a γ-secretase inhibitor, has
525 shown promise as a potential therapeutic target for many conditions ranging from cancer
526 to cardiovascular diseases. DAPT promotes cardiac reprogramming and has been
527 suggested as a potential therapeutic option for cardiac regeneration[48]. In this study, we
528 show that DAPT prevents cardiac dysfunction in ISO+sFRP1-treated rats. These findings
529 provide not only mechanistic insight into DCM in children but also a potential therapeutic
530 target for pediatric DCM.

531

532 **Cardiac stiffness as a characteristic of pediatric DCM**

533 Additionally, our *in vivo* model recapitulates other aspects of pediatric DCM, such as no
534 difference in cardiac *NPPB* levels, minimal fibrosis or lack of myocyte hypertrophy[8,17].
535 While fibrosis was not observed in our model, we detected an increase in myocardial
536 stiffness, which recapitulates our prior *in vitro* studies in cells treated with sFRP1[12].
537 Notably, both WNT and Notch signaling have been implicated in the regulation of
538 extracellular matrix dynamics and fibroblast activation in adult cardiac fibrosis[49]; however,

539 in pediatric iDCM, our transcriptomic data suggest these pathways may instead contribute
540 to cardiomyocyte-intrinsic changes and ECM remodeling resulting in stiffness in the
541 absence of classical interstitial fibrosis. The enrichment of ECM pathways in our rat model
542 aligns with this observation and supports the idea that pediatric iDCM may involve
543 dynamic ECM dysregulation without overt fibrotic conversion. Also, ECM remodeling in
544 the absence of overt fibrosis may represent a unique pathogenic mechanism underlying
545 pediatric iDCM. ECM remodeling and myocardial stiffness have been detected in the
546 hearts of children with iDCM[5,26]. Our results expand on these prior findings and show that
547 stiffness is increased in pediatric iDCM hearts by AFM and may contribute to impaired
548 cardiac function. ECM stiffness is an important cue that usually precedes fibrosis and can
549 act through WNT signaling[50]. In addition, modulation of Notch signaling regulates
550 substrate stiffness associated with stiffness of the ECM via mechanotransduction[41], and
551 may explain the lack of fibrosis but presence of stiffness in pediatric iDCM. Taken
552 together, our findings suggest myocardial stiffness as an important contributor to pediatric
553 iDCM and support WNT and Notch signaling pathways as important drivers of the disease
554 in children.

555

556 **CONCLUSION**

557 Our study identified a novel paradigm in the investigations of pediatric iDCM that consists
558 of a combined activation of WNT and Notch pathways. Through *in vitro* studies, we
559 established the secretome as an important mediator of disease, which led to the
560 development of an *in vivo* model of pediatric iDCM. Using this model, we identified co-
561 activation of Notch and WNT in ISO+sFRP1-treated rats and human pediatric iDCM

562 tissue. Mechanistically, *in vitro* inhibition of Notch and β-catenin signaling prevented
563 pathological remodeling, and *in vivo* Notch inhibition improved cardiac function. These
564 results emphasize the relevance of our model for studying pediatric-specific mechanisms
565 of HF and suggest that targeting the Notch–WNT axis could offer new therapeutic
566 opportunities. Collectively, our findings provide an opportunity to explore potential novel
567 therapeutic targets in pediatric DCM.

568

569 **LIMITATIONS**

570 (1) This study focused on a young model of disease and its relationship to the pediatric
571 heart. Adults were not included in our analysis. (2) The increase in myocardial stiffness
572 justifies the need to explore the potential mechanisms underlying this increase in
573 stiffness. Understanding the processes associated with ECM remodeling will further our
574 understanding of iDCM mechanisms in children and may identify novel approaches to
575 prevent or reverse stiffness. (3) Although our studies suggest Notch inhibition may be a
576 sound approach to prevent the disease process, the effect of inhibiting β-catenin is yet to
577 be investigated. (4) The current study focused on the interplay between β-catenin and
578 Notch. However, other pathways identified in our transcriptomic data may be relevant and
579 can be further explored in future studies.

580

581 **METHODS**

582 Detailed methods can be found in the Supplemental Materials.

583

584 **Author contributions**

585 OON performed experiments, data analysis and interpretation, manuscript writing and
586 editing. ER performed experiments, data analysis and manuscript writing. JG performed
587 experiments and data analysis. AKF performed statistical and bioinformatics analyses.
588 CC performed some experiments. LHL performed experiments, MPAB performed data
589 analysis. BP performed experiments and guided AFM analysis. SDM was involved in
590 experimental design, project supervision, clinical data interpretation, and manuscript
591 writing and editing. BLS was involved in experimental design, project supervision, data
592 interpretation, and manuscript writing and editing. CCS conceptualized the study, was
593 involved in experimental design, data analysis and interpretation, manuscript writing and
594 editing. All authors reviewed and approved the manuscript.
595

596 **Acknowledgments**

597 We would like to acknowledge the Heart Transplant Team at Children's Hospital
598 Colorado.
599 We would also like to acknowledge the University of Colorado hemodynamics core,
600 especially Elizabeth Hardy, for taking all echocardiographic measurements. Finally, we
601 are grateful to the Integrated Physiology Program at the University of Colorado,
602 particularly Dr. Mary Weiser-Evans, the program Director.
603

604 **Sources of Funding**

605 This work was supported by NIH K24HL150630 (to CCS), the Colorado CTSA Grant (UL1
606 TR002535), NIH R01HL156670 (to SDM, BLS, CCS), the Jack Cooper Millisor Chair in
607 Pediatric Heart Disease (to SDM), American Heart Association (AHA) supplement to
608 promote diversity in science (24DIVSUP1281949) (to OON), AHA predoctoral fellowship

609 (25PRE1375864) (to OON), NIH K25HL148386 (to BP), the Ludeman Family Center for
610 Women's Health Research seed grant (to BP), American Heart Association
611 23CDA1052411 (to BP) and the generous grants of John Patrick Albright (to BP).

612

613 **Disclosure of interest**

614 None of the authors have a conflict of interest

615 **Data availability statement**

616 Bulk and single-nucleus RNA sequencing data will be deposited upon acceptance of the
617 manuscript.

618 **References**

619 1. Shaddy RE, Boucek MM, Hsu DT, et al. Carvedilol for Children and Adolescents With
620 Heart Failure: A Randomized Controlled Trial. *JAMA*. 2007;298(10):1171-1179.
621 doi:10.1001/JAMA.298.10.1171
622 2. Lefkowitz RJ, Rockman HA, Koch WJ. Catecholamines, Cardiac β-Adrenergic Receptors,
623 and Heart Failure. *Circulation*. 2000;101(14):1634-1637. doi:10.1161/01.CIR.101.14.1634
624 3. Venugopalan P, Agarwal AK. Plasma catecholamine levels parallel severity of heart failure
625 and have prognostic value in children with dilated cardiomyopathy. *Eur J Heart Fail*.
626 2003;5(5):655-658. doi:10.1016/S1388-9842(03)00109-0
627 4. Quiat D, Witkowski L, Zouk H, Daly KP, Roberts AE. Retrospective Analysis of Clinical
628 Genetic Testing in Pediatric Primary Dilated Cardiomyopathy: Testing Outcomes and the
629 Effects of Variant Reclassification. *J Am Heart Assoc*. 2020;9(11).
630 doi:10.1161/JAHA.120.016195

631 5. Patel MD, Mohan J, Schneider C, et al. Pediatric and adult dilated cardiomyopathy
632 represent distinct pathological entities. *JCI Insight*. 2017;2(14).
633 doi:10.1172/JCI.INSIGHT.94382
634 6. Lee TM, Hsu DT, Kantor P, et al. Pediatric Cardiomyopathies. *Circ Res*. 2017;121(7):855-
635 873. doi:10.1161/CIRCRESAHA.116.309386
636 7. Woulfe KC, Siomos AK, Nguyen H, et al. Fibrosis and Fibrotic Gene Expression in Pediatric
637 and Adult Patients With Idiopathic Dilated Cardiomyopathy. *J Card Fail*. 2017;23(4):314-
638 324. doi:10.1016/J.CARDFAIL.2016.11.006
639 8. Tatman PD, Woulfe KC, Karimpour-Fard A, et al. Pediatric dilated cardiomyopathy hearts
640 display a unique gene expression profile. *JCI Insight*. 2017;2(14).
641 doi:10.1172/JCI.INSIGHT.94249
642 9. Miyamoto SD, Stauffer BL, Nakano S, et al. Editor's choice: Beta-adrenergic adaptation in
643 paediatric idiopathic dilated cardiomyopathy. *Eur Heart J*. 2014;35(1):33.
644 doi:10.1093/EURHEARTJ/EHS229
645 10. Taegtmeyer H, Sen S, Vela D. Return to the fetal gene program: A suggested metabolic
646 link to gene expression in the heart. *Ann N Y Acad Sci*. 2010;1188:191.
647 doi:10.1111/J.1749-6632.2009.05100.X
648 11. Nyarko OO, Sucharov CC. The secretome as a biomarker and functional agent in heart
649 failure. *J Cardiovasc Aging 2023;3:27*. 2023;3(3):N/A-N/A. doi:10.20517/JCA.2023.15
650 12. Jeffrey DA, da Silva JP, Garcia AM, et al. Serum circulating proteins from pediatric
651 patients with dilated cardiomyopathy cause pathologic remodeling and cardiomyocyte
652 stiffness. *JCI Insight*. 2021;6(19). doi:10.1172/JCI.INSIGHT.148637

653 13. Liang CJ, Wang ZW, Chang YW, Lee KC, Lin WH, Lee JL. SFRPs Are Biphasic Modulators of
654 Wnt-Signaling-Elicited Cancer Stem Cell Properties beyond Extracellular Control. *Cell Rep*.
655 2019;28(6):1511-1525.e5. doi:10.1016/J.CELREP.2019.07.023
656 14. Gao J, Fan L, Zhao L, Su Y. The interaction of Notch and Wnt signaling pathways in
657 vertebrate regeneration. *Cell Regeneration 2021 10:1*. 2021;10(1):1-17.
658 doi:10.1186/S13619-020-00072-2
659 15. Fre S, Pallavi SK, Huyghe M, et al. Notch and Wnt signals cooperatively control cell
660 proliferation and tumorigenesis in the intestine. *Proc Natl Acad Sci U S A*.
661 2009;106(15):6309. doi:10.1073/PNAS.0900427106
662 16. Quillard T, Charreau B. Impact of Notch Signaling on Inflammatory Responses in
663 Cardiovascular Disorders. *International Journal of Molecular Sciences 2013, Vol 14, Pages*
664 *6863-6888*. 2013;14(4):6863-6888. doi:10.3390/IJMS14046863
665 17. Woulfe KC, Siomos AK, Nguyen H, et al. Fibrosis and Fibrotic Gene Expression in Pediatric
666 and Adult Patients With Idiopathic Dilated Cardiomyopathy. *J Card Fail*. 2017;23(4):314-
667 324. doi:10.1016/J.CARDFAIL.2016.11.006
668 18. Koenig AL, Shchukina I, Amrute J, et al. Single-cell transcriptomics reveals cell-type-
669 specific diversification in human heart failure. *Nature cardiovascular research*.
670 2022;1(3):263-280. doi:10.1038/S44161-022-00028-6
671 19. Amrute JM, Lai L, Ma P, et al. Defining cardiac functional recovery in end-stage heart
672 failure at single-cell resolution. *Nature cardiovascular research*. 2023;2(4):399.
673 doi:10.1038/S44161-023-00260-8

674 20. Ueno S, Weidinger G, Osugi T, et al. Biphasic role for Wnt/β-catenin signaling in cardiac
675 specification in zebrafish and embryonic stem cells. *Proc Natl Acad Sci U S A*.
676 2007;104(23):9685. doi:10.1073/PNAS.0702859104
677 21. Kumar V, Vashishta M, Kong L, et al. The Role of Notch, Hedgehog, and Wnt Signaling
678 Pathways in the Resistance of Tumors to Anticancer Therapies. *Front Cell Dev Biol*.
679 2021;9:650772. doi:10.3389/FCELL.2021.650772
680 22. Galceran J, Sustmann C, Hsu SC, Folberth S, Grosschedl R. LEF1-mediated regulation of
681 Delta-like1 links Wnt and Notch signaling in somitogenesis. *Genes Dev*.
682 2004;18(22):2718. doi:10.1101/GAD.1249504
683 23. Singh RK, Canter CE, Shi L, et al. Survival Without Cardiac Transplantation Among
684 Children With Dilated Cardiomyopathy. *J Am Coll Cardiol*. 2017;70(21):2663-2673.
685 doi:10.1016/J.JACC.2017.09.1089
686 24. Loss KL, Shaddy RE, Kantor PF. Recent and Upcoming Drug Therapies for Pediatric Heart
687 Failure. *Front Pediatr*. 2021;9:11. doi:10.3389/FPED.2021.681224
688 25. Aisagbonhi O, Rai M, Ryzhov S, Atria N, Feoktistov I, Hatzopoulos AK. Experimental
689 myocardial infarction triggers canonical Wnt signaling and endothelial-to-mesenchymal
690 transition. *Dis Model Mech*. 2011;4(4):469-483. doi:10.1242/DMM.006510
691 26. Regel I, Eichenmüller M, Mahajan UM, et al. Downregulation of SFRP1 is a
692 protumorigenic event in hepatoblastoma and correlates with beta-catenin mutations. *J
693 Cancer Res Clin Oncol*. 2020;146(5):1153-1167. doi:10.1007/S00432-020-03182-
694 1/TABLES/2

695 27. Lin XH, Liu HH, Hsu SJ, et al. Norepinephrine-stimulated HSCs secrete sFRP1 to promote
696 HCC progression following chronic stress via augmentation of a Wnt16B/β-catenin
697 positive feedback loop. *J Exp Clin Cancer Res*. 2020;39(1). doi:10.1186/S13046-020-
698 01568-0
699 28. Bu Q, Li Z, Zhang J, Xu F, Liu J, Liu H. The crystal structure of full-length Sizzled from
700 Xenopus laevis yields insights into Wnt-antagonistic function of secreted Frizzled-related
701 proteins. *Journal of Biological Chemistry*. 2017;292(39):16055-16069.
702 doi:10.1074/JBC.M117.791756
703 29. Cheng LC, Chao YJ, Overman MJ, et al. Increased expression of secreted frizzled related
704 protein 1 (SFRP1) predicts ampullary adenocarcinoma recurrence. *Scientific Reports 2020*
705 *10:1*. 2020;10(1):1-16. doi:10.1038/s41598-020-69899-8
706 30. Horitani K, Shiojima I. Wnt signaling in cardiac development and heart diseases. *In Vitro*
707 *Cell Dev Biol Anim*. 2024;60(5):482. doi:10.1007/S11626-024-00917-Z
708 31. Tseng AS, Engel FB, Keating MTT. The GSK-3 inhibitor BIO promotes proliferation in
709 mammalian cardiomyocytes. *Chem Biol*. 2006;13(9):957-963.
710 doi:10.1016/J.CHEMBIOL.2006.08.004
711 32. Chen X, Shevtsov SP, Hsich E, et al. The β-Catenin/T-Cell Factor/Lymphocyte Enhancer
712 Factor Signaling Pathway Is Required for Normal and Stress-Induced Cardiac
713 Hypertrophy. *Mol Cell Biol*. 2006;26(12):4462. doi:10.1128/MCB.02157-05
714 33. Oerlemans MIFJ, Goumans MJ, Van Middelaar B, Clevers H, Doevendans PA, Sluijter JPG.
715 Active Wnt signaling in response to cardiac injury. *Basic Res Cardiol*. 2010;105(5):631-
716 641. doi:10.1007/S00395-010-0100-9/FIGURES/6

717 34. Baurand A, Zelarayan L, Betney R, et al. Beta-catenin downregulation is required for
718 adaptive cardiac remodeling. *Circ Res*. 2007;100(9):1353-1362.
719 doi:10.1161/01.RES.0000266605.63681.5A
720 35. Collu GM, Hidalgo-Sastre A, Brennan K. Wnt–Notch signalling crosstalk in development
721 and disease. *Cell Mol Life Sci*. 2014;71(18):3553. doi:10.1007/S00018-014-1644-X
722 36. Ruijmbeek CWB, Housley F, Idrees H, et al. Biallelic variants in FLII cause pediatric
723 cardiomyopathy by disrupting cardiomyocyte cell adhesion and myofibril organization.
724 *JCI Insight*. 2023;8(17):e168247. doi:10.1172/JCI.INSIGHT.168247
725 37. Fischer A, Schumacher N, Maier M, Sendtner M, Gessler M. The Notch target genes Hey1
726 and Hey2 are required for embryonic vascular development. *Genes Dev*. 2004;18(8):901.
727 doi:10.1101/GAD.291004
728 38. Niessen K, Karsan A. Notch signaling in cardiac development. *Circ Res*.
729 2008;102(10):1169-1181. doi:10.1161/CIRCRESAHA.108.174318/ASSET/D2E086FF-4E20-
730 4858-A7B0-4F339541366A/ASSETS/GRAPHIC/9FF4.JPEG
731 39. Li Y, Hiroi Y, Liao JK. Notch Signaling as an Important Mediator of Cardiac Repair and
732 Regeneration after Myocardial Infarction. *Trends Cardiovasc Med*. 2010;20(7):228.
733 doi:10.1016/J.TCM.2011.11.006
734 40. Li H, Chang C, Li X, Zhang R. The roles and activation of endocardial Notch signaling in
735 heart regeneration. *Cell Regeneration*. 2021;10(1). doi:10.1186/S13619-020-00060-6
736 41. Kretschmer M, Mamistvalov R, Sprinzak D, Vollmar AM, Zahler S. Matrix stiffness
737 regulates Notch signaling activity in endothelial cells. *J Cell Sci*. 2023;136(2).
738 doi:10.1242/JCS.260442/286810

739 42. Collesi C, Zentilin L, Sinagra G, Giacca M. Notch1 signaling stimulates proliferation of
740 immature cardiomyocytes. *Journal of Cell Biology*. 2008;183(1):117-128.
741 doi:10.1083/JCB.200806091
742 43. Pećina-Šlaus N. Wnt signal transduction pathway and apoptosis: a review. *Cancer Cell Int*.
743 2010;10:22. doi:10.1186/1475-2867-10-22
744 44. Wang Y, Lu P, Wu B, Morrow BE, Zhou B. NOTCH maintains developmental cardiac gene
745 network through WNT5A. *J Mol Cell Cardiol*. 2018;125:98.
746 doi:10.1016/J.YJMCC.2018.10.014
747 45. Malekar P, Hagenmueller M, Anyanwu A, et al. Wnt signaling is critical for maladaptive
748 cardiac hypertrophy and accelerates myocardial remodeling. *Hypertension*.
749 2010;55(4):939-945. doi:10.1161/HYPERTENSIONAHA.109.141127
750 46. Kwon C, Cheng P, King IN, et al. Notch Post-Translationally Regulates β-Catenin Protein in
751 Stem and Progenitor Cells. *Nat Cell Biol*. 2011;13(10):1244. doi:10.1038/NCB2313
752 47. Adu-Amankwaah J, Adzika GK, Adekunle AO, et al. ADAM17, A Key Player of Cardiac
753 Inflammation and Fibrosis in Heart Failure Development During Chronic Catecholamine
754 Stress. *Front Cell Dev Biol*. 2021;9. doi:10.3389/FCELL.2021.732952
755 48. Abad M, Hashimoto H, Zhou H, et al. Notch Inhibition Enhances Cardiac Reprogramming
756 by Increasing MEF2C Transcriptional Activity. *Stem Cell Reports*. 2017;8(3):548.
757 doi:10.1016/J.STEMCR.2017.01.025
758 49. Docshin P, Panshin D, Malashicheva A. Molecular Interplay in Cardiac Fibrosis: Exploring
759 the Functions of RUNX2, BMP2, and Notch. *Rev Cardiovasc Med*. 2024;25(10):368.
760 doi:10.31083/J.RCM2510368

761 50. He J, Cheng X, Fang B, Shan S, Li Q. Mechanical stiffness promotes skin fibrosis via Piezo1-
762 Wnt2/Wnt11-CCL24 positive feedback loop. *Cell Death & Disease 2024 15:1*.
763 2024;15(1):1-14. doi:10.1038/s41419-024-06466-3

764

765

766 **FIGURES AND LEGENDS**

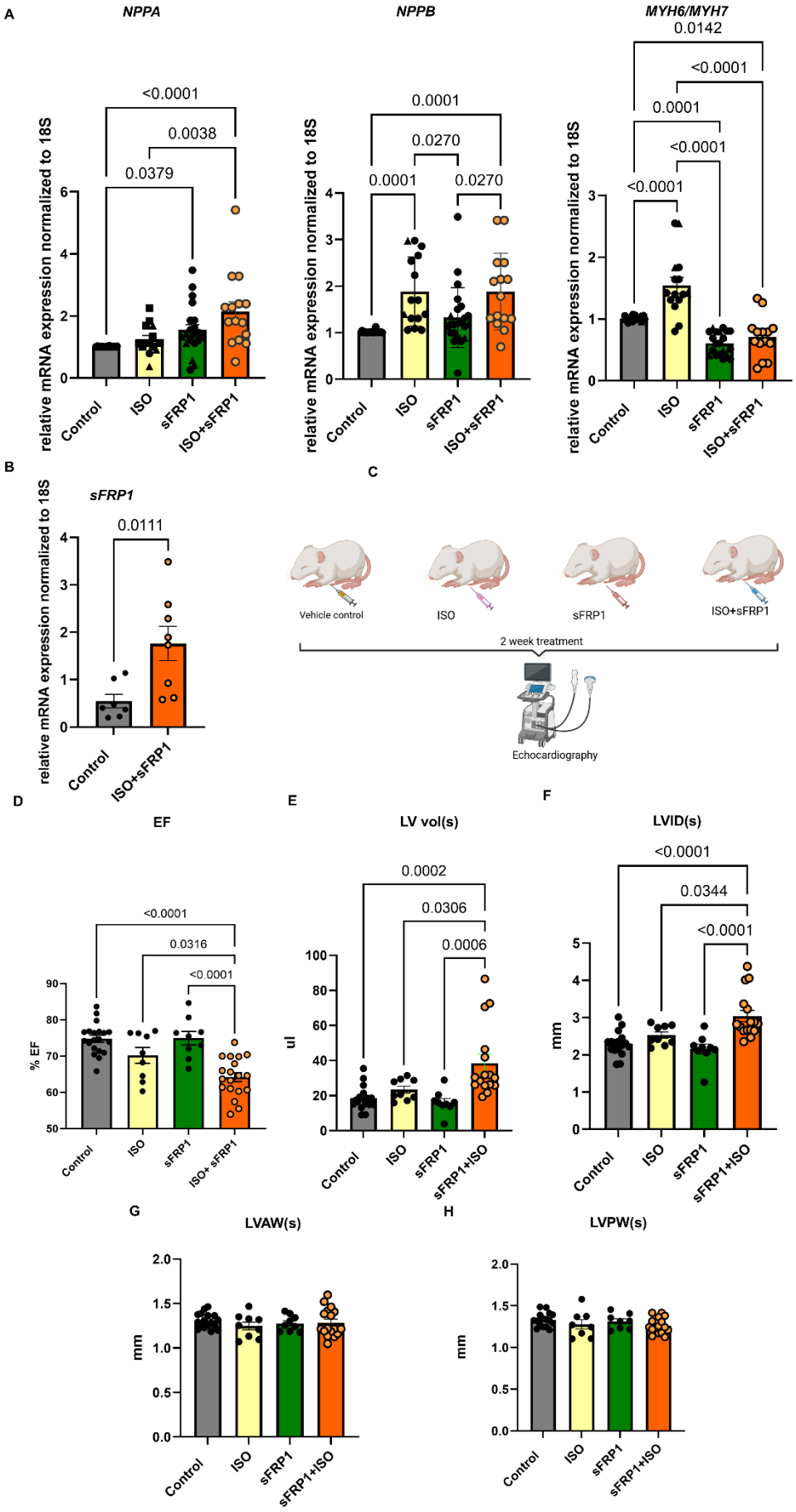
A
NPPA
NPPB
MYH6/MYH7
relative mRNA expression normalized to 18S
<0.0001
0.0038
0.0379
0.0001
0.0270
0.0142
Control
ISO
sFRP1
ISO+sFRP1
B
sFRP1
0.0111
C
Vehicle control
ISO
sFRP1
ISO+sFRP1
2 week treatment
Echocardiography
D
EF
% EF
E
LV vol(s)
ul
0.0002
0.0306
0.0006
F
LVID(s)
mm
0.0344
G
LVAW(s)
H
LVPW(s)
sFRP1+ISO

768 Figure 1. ISO+sFRP1 promotes pathological remodeling in NRVMs and cardiac
769 dysfunction *in vivo*.

770 (A) RT-qPCR of FGP expression in NRVMs treated with vehicle (Control), ISO,
771 sFRP1 or ISO+sFRP1. Expression of *NPPA*, *NPPB*, and ratio of *MYH6* to *MYH7*.
772 Gene expression was normalized to 18S, and data are presented as a relative
773 fold change to Controls. NRVMs treated with 100nM Isoproterenol (ISO) +/- 1
774 µg/mL human recombinant sFRP1 for 72 hours. *n* = 8 independent NRVM preps.
775 All groups are log2 transformed.

776 (B) RT-qPCR of sFRP1 gene expression in NRVMs treated with ISO+sFRP1
777 compared to vehicle-treated controls. Gene expression was normalized to 18S,
778 and data are presented as a relative fold change to controls. *n* = 6 independent
779 NRVM preps.

780 (C) Schematic of injection plan, timeline and duration. Rats were treated with
781 0.1mg/kg/day ISO every other day for the first 5 treatments and every day for the
782 subsequent 7 days. sFRP1 (50µg/kg/day) was co-administered with ISO (or
783 vehicle (PBS, 0.5mM ascorbic acid).

784 (D) EF of neonatal rats treated with vehicle (Control), ISO, sFRP1 and ISO+sFRP1.

785 (E) LV vol(s) of neonatal rats treated with vehicle (Control), ISO, sFRP1 and
786 ISO+sFRP1.

787 (F) LVID(s) of neonatal rats treated with vehicle (Control), ISO, sFRP1 and
788 ISO+sFRP1.

789 (G) LVAW(s) of neonatal rats treated with vehicle (Control), ISO, sFRP1 and
790 ISO+sFRP1.

791 (H) LVPW(s) of neonatal rats treated with vehicle (Control), ISO, sFRP1 and
792 ISO+sFRP1.

793 Control *n* = 20, ISO *n* = 9, sFRP1 *n* = 9, ISO+sFRP1 *n*=19. Only significant *p*-
794 values are notated in the Figure.

795 Only significant *P* values (p<0.05) are notated in the Figure. Fitting a mixed
796 model, Tukey's multiple comparisons test was used for multiple comparison.
797 Unpaired *t*-test was used for two-group analysis. Error bar denotes mean± SEM.
798 NRVMs, neonatal rat ventricular myocytes; FGP, fetal gene program; ISO,
799 Isoproterenol; sFRP1, secreted frizzled protein 1; EF, ejection fraction; LV vol(s),
800 Left ventricular volume in systole; LVID. Left ventricular internal diameter in
801 systole; LVAW(s), left ventricular anterior wall in systole; LVPW (s), left
802 ventricular posterior wall in systole.

803

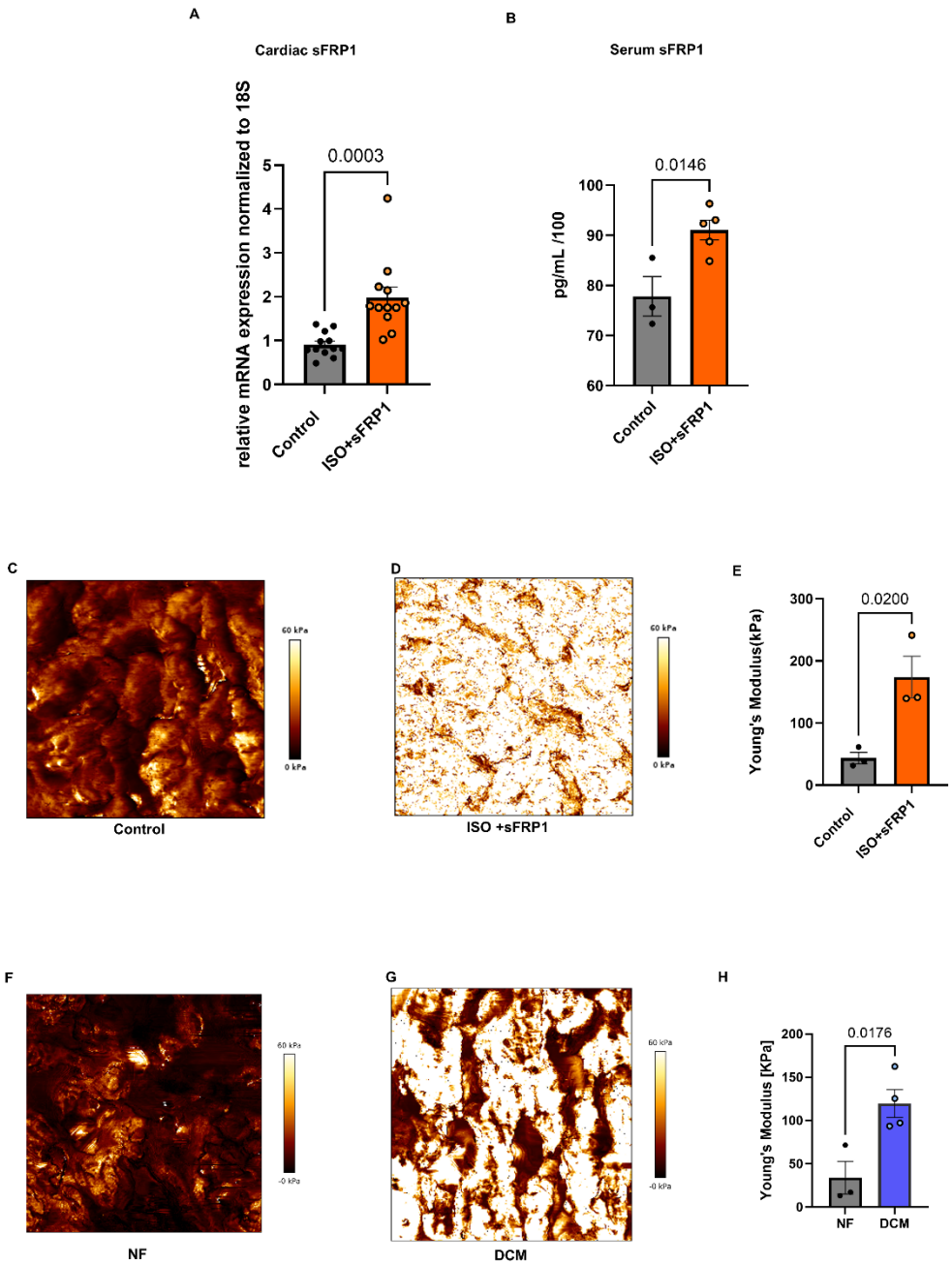
A
Cardiac sFRP1
relative mRNA expression normalized to 18S
0.0003
Control
ISO+sFRP1
B
Serum sFRP1
pg/mL /100
0.0146
Control
ISO+sFRP1
C
60 kPa
0 kPa
Control
D
60 kPa
0 kPa
ISO +sFRP1
E
Young's Modulus(kPa)
0.0200
Control
ISO+sFRP1
F
60 kPa
-0 kPa
NF
G
60 kPa
-0 kPa
DCM
H
Young's Modulus [KPa]
0.0176
NF
DCM

805 Figure 2. Cardiac stiffness is increased in pediatric DCM hearts and ISO+sFRP1 rats.

806 (A) Levels of sFRP1 mRNA in left ventricle (LV) tissue of ISO+sFRP1-treated rats
807 compared to controls. Gene expression was measured by RT-qPCR and
808 normalized to 18S. *n* = 12/group. Data are presented as a relative fold change to
809 NF controls; all data are log2 transformed.

810 (B) Levels of sFRP1 in serum from ISO+sFRP1 rats compared to controls. Serum
811 levels were measured by ELISA. Control *n* = 3, ISO+sFRP1 *n* = 5. ELISA,
812 Enzyme-linked immunosorbent assay.

813 (C-E) Elasticity/stiffness (Young's modulus) in rats treated with ISO+sFRP1 (D)
814 compared to controls (C). Quantification is shown in (E). *n* =3 per group.

815 (F-H) Elasticity/stiffness (Young's modulus) in explanted pediatric DCM hearts (G)
816 compared to non-failing controls (F). Quantification is shown in (H). NF *n* =3,
817 DCM *n =4*.

818 Unpaired 2-tailed *t*-test was used in all analyses. Only Significant *p*-values
819 ($p<0.05$) are notated in the Figure. Error bar denotes mean ± SEM. NF, non-
820 failing; DCM, dilated cardiomyopathy

821

A

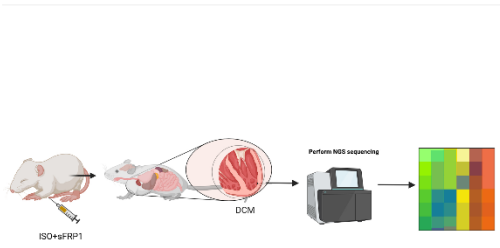
ISO+sFRP1
DCM
Perform NGS sequencing

B

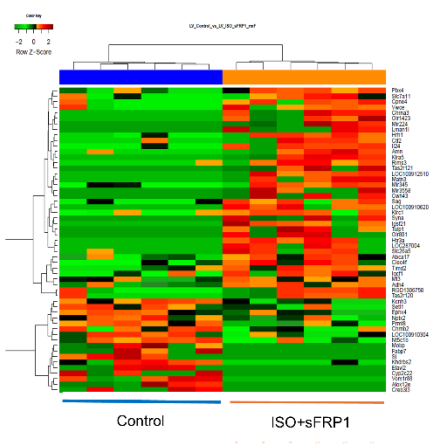
Row Z-Score
Control
ISO+sFRP1

C

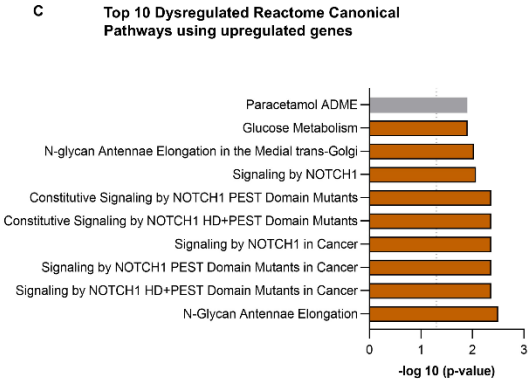
Top 10 Dysregulated Reactome Canonical Pathways using upregulated genes
Paracetamol ADME
Glucose Metabolism
N-glycan Antennae Elongation in the Medial trans-Golgi
Signaling by NOTCH1
Constitutive Signaling by NOTCH1 PEST Domain Mutants
Constitutive Signaling by NOTCH1 HD+PEST Domain Mutants
Signaling by NOTCH1 in Cancer
Signaling by NOTCH1 PEST Domain Mutants in Cancer
Signaling by NOTCH1 HD+PEST Domain Mutants in Cancer
N-Glycan Antennae Elongation
0
1
2
3
-log 10 (p-value)

D

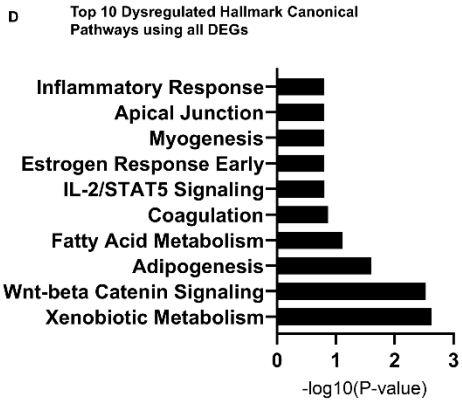
Top 10 Dysregulated Hallmark Canonical Pathways using all DEGs
Inflammatory Response
Apical Junction
Myogenesis
Estrogen Response Early
IL-2/STAT5 Signaling
Coagulation
Fatty Acid Metabolism
Adipogenesis
Wnt-beta Catenin Signaling
Xenobiotic Metabolism
0
1
2
3
-log10(P-value)

E

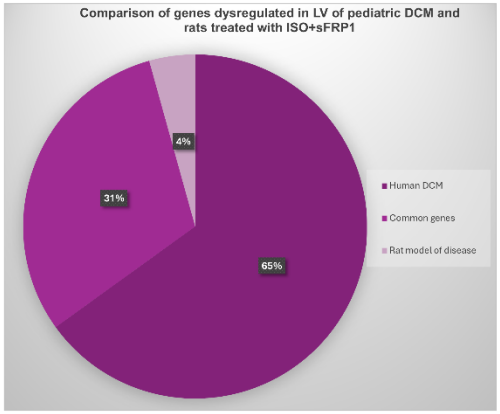
Comparison of genes dysregulated in LV of pediatric DCM and rats treated with ISO+sFRP1
4%
31%
65%
Human DCM
Common genes
Rat model of disease

F

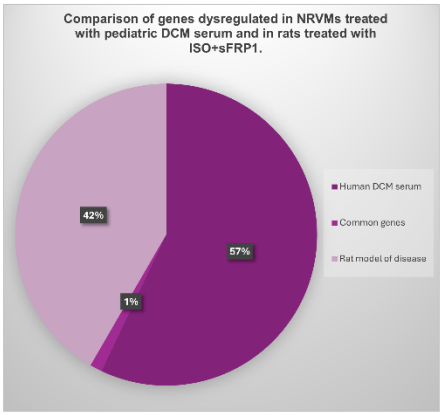
Comparison of genes dysregulated in NRVMs treated with pediatric DCM serum and in rats treated with ISO+sFRP1.
42%
57%
1%
Human DCM serum
Common genes
Rat model of disease

G

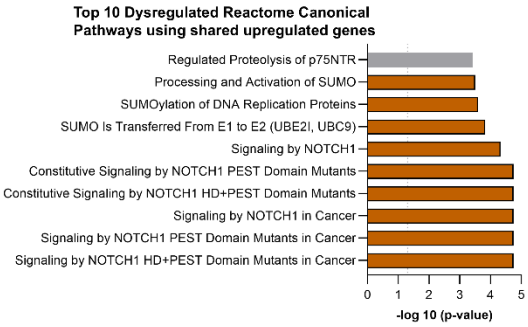
Top 10 Dysregulated Reactome Canonical Pathways using shared upregulated genes
Regulated Proteolysis of p75NTR
Processing and Activation of SUMO
SUMOylation of DNA Replication Proteins
SUMO Is Transferred From E1 to E2 (UBE2I, UBC9)
Signaling by NOTCH1
Constitutive Signaling by NOTCH1 PEST Domain Mutants
Constitutive Signaling by NOTCH1 HD+PEST Domain Mutants
Signaling by NOTCH1 in Cancer
Signaling by NOTCH1 PEST Domain Mutants in Cancer
Signaling by NOTCH1 HD+PEST Domain Mutants in Cancer
0
1
2
3
4
5
-log 10 (p-value)

823 Figure 3. Notch and WNT signaling are predicted to be altered in ISO+sFRP1 rats and
824 in pediatric DCM hearts.

825 (A) Schematic of the experimental plan and bulk RNA-sequencing.

826 (B) Heatmap representing unsupervised hierarchical clustering of the top 50
827 significantly differentially expressed genes (DEGs). n = 6/group; Welch's t test p
828 < 0.05.

829 (C) Pathway analysis using the 113 upregulated genes in ISO+sFRP1 vs Control rats
830 using Reactome pathway analysis tool.

831 (D) Pathway analysis using all 286 differentially expressed genes in ISO+sFRP1 vs
832 Control rats using Hallmark pathway analysis tool.

833 (E) Venn diagram representation of overlapping genes altered in pediatric DCM left
834 ventricle (LV) tissue compared to non-failing controls, and in LV tissue from
835 ISO+sFRP1-treated rats compared to controls.

836 (F) Venn diagram representation of overlapping genes altered in pediatric DCM
837 serum-treated NRVMs compared to cells treated with serum from age-matched
838 non-failing controls, and in LV tissue from ISO+sFRP1-treated rats compared to
839 controls.

840 (G) Pathway analysis using the upregulated genes shared in serum-treated NRVMs
841 and LV tissue of ISO+sFRP1-treated rats identified by Reactome pathway
842 analysis tool.

843 DCM, dilated cardiomyopathy; ISO-Isoproterenol, sFRP1- secreted frizzled
844 protein 1; NRVMs, neonatal rat ventricular myocytes; LV, left ventricle.

845

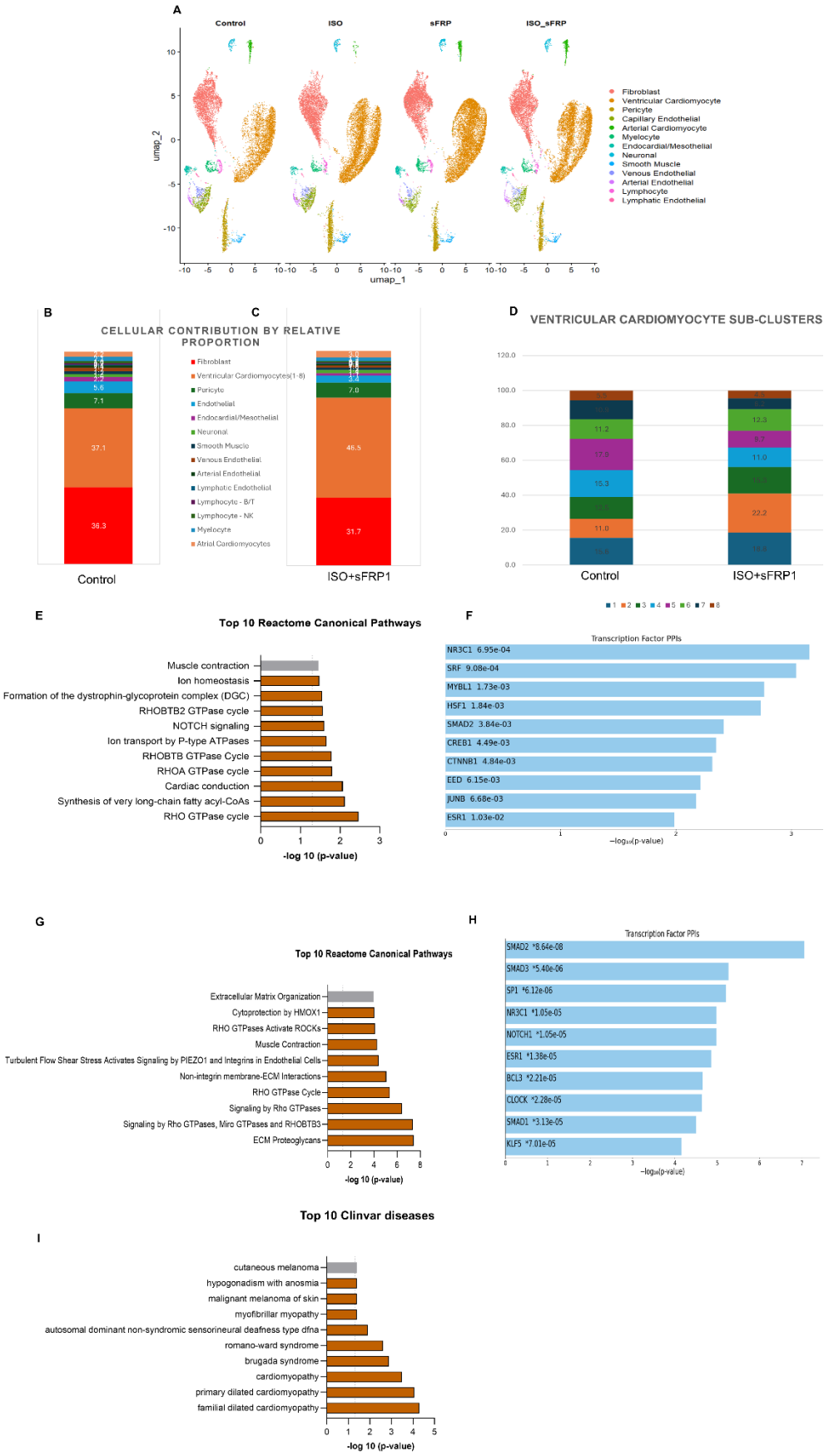
A
Control
ISO
sFRP
ISO_sFRP
umap_2
umap_1
Fibroblast
Ventricular Cardiomyocyte
Pericyte
Capillary Endothelial
Arterial Cardiomyocyte
Myelocyte
Endocardial/Mesothelial
Neuronal
Smooth Muscle
Venous Endothelial
Arterial Endothelial
Lymphocyte
Lymphatic Endothelial
B
C
CELLULAR CONTRIBUTION BY RELATIVE PROPORTION
Fibroblast
Ventricular Cardiomyocytes(1-8)
Pericyte
Endothelial
Endocardial/Mesothelial
Neuronal
Smooth Muscle
Venous Endothelial
Arterial Endothelial
Lymphatic Endothelial
Lymphocyte - B/T
Lymphocyte - NK
Myelocyte
Atrial Cardiomyocytes
Control
ISO+sFRP1
D
VENTRICULAR CARDIOMYOCYTE SUB-CLUSTERS
Control
ISO+sFRP1
E
Top 10 Reactome Canonical Pathways
Muscle contraction
Ion homeostasis
Formation of the dystrophin-glycoprotein complex (DGC)
RHOBTB2 GTPase cycle
NOTCH signaling
Ion transport by P-type ATPases
RHOBTB GTPase Cycle
RHOA GTPase cycle
Cardiac conduction
Synthesis of very long-chain fatty acyl-CoAs
RHO GTPase cycle
-log 10 (p-value)
F
Transcription Factor PPIs
NR3C1 6.95e-04
SRF 9.08e-04
MYBL1 1.73e-03
HSF1 1.84e-03
SMAD2 3.84e-03
CREB1 4.49e-03
CTNNB1 4.84e-03
EED 6.15e-03
JUNB 6.68e-03
ESR1 1.03e-02
G
Top 10 Reactome Canonical Pathways
Extracellular Matrix Organization
Cytoprotection by HMOX1
RHO GTPases Activate ROCKs
Muscle Contraction
Turbulent Flow Shear Stress Activates Signaling by PIEZO1 and Integrins in Endothelial Cells
Non-integrin membrane-ECM Interactions
RHO GTPase Cycle
Signaling by Rho GTPases
Signaling by Rho GTPases, Miro GTPases and RHOBTB3
ECM Proteoglycans
-log 10 (p-value)
H
Transcription Factor PPIs
SMAD2 *8.64e-08
SMAD3 *5.40e-06
SP1 *6.12e-06
NR3C1 *1.05e-05
NOTCH1 *1.05e-05
ESR1 *1.38e-05
BCL3 *2.21e-05
CLOCK *2.28e-05
SMAD1 *3.13e-05
KLF5 *7.01e-05
I
Top 10 Clinvar diseases
cutaneous melanoma
hypogonadism with anosmia
malignant melanoma of skin
myofibrillar myopathy
autosomal dominant non-syndromic sensorineural deafness type dfna
romano-ward syndrome
brugada syndrome
cardiomyopathy
primary dilated cardiomyopathy
familial dilated cardiomyopathy
-log 10 (p-value)

846

847 Figure 4. Single-nuclei RNA sequencing (snRNA-seq) identifies activation of Notch and
848 β-catenin signaling in response to ISO+sFPR1.
849 (A) Representative UMAP plot from single-nuclei RNA sequencing of LV tissue from
850 Controls, ISO-, sFRP1- or ISO+sFRP1-treated rats, *n* = 3/group. A total of 9214
851 nuclei in control, 11588 nuclei in ISO-, 13758 nuclei in sFRP1-, and 11127 in
852 ISO+sFRP1-treated rats were identified after cells were pooled. 26 distinct cell
853 clusters were identified including 8 CMs and 5 FBs.
854 (B) Graphical representation of the percent cell type distribution in vehicle-treated
855 control rats.
856 (C) Graphical representation of the percent cell type distribution in ISO+sFRP1 rats.
857 (D) Graphical representation of the percent ventricular cardiomyocyte sub-clusters in
858 vehicle-treated control rats and ISO+sFRP1.
859 (E) Reactome pathway analysis using upregulated genes in Ventricular
860 cardiomyocyte sub-cluster 2 of ISO+sFRP1 vs Control rats.
861 (F) Enrichr analysis identifies transcription factors predicted to control expression of
862 upregulated genes in ventricular cardiomyocyte sub-cluster 2.
863 (G) Reactome pathways analysis using upregulated genes in ventricular
864 cardiomyocyte sub-cluster 6 of ISO+sFRP1 vs Control rats.
865 (H) Enrichr analysis identifies transcription factors predicted to control expression of
866 upregulated genes in ventricular cardiomyocyte sub-cluster 6.
867 (I) ClinVar database analysis of upregulated genes in the ventricular cardiomyocyte
868 cluster.
869 Clusters were annotated into major cell populations, and the ventricular
870 cardiomyocyte cluster was sub-clustered into eight different sub-clusters using R

871 statistical software. Differentially expressed genes for each cluster were calculated
872 with the FindAllMarkers function. UMAP: uniform manifold approximation and
873 projection, CM: cardiomyocytes; FB: fibroblast; NK: Natural Killer cells; B/T: B cells
874 and T cells
875

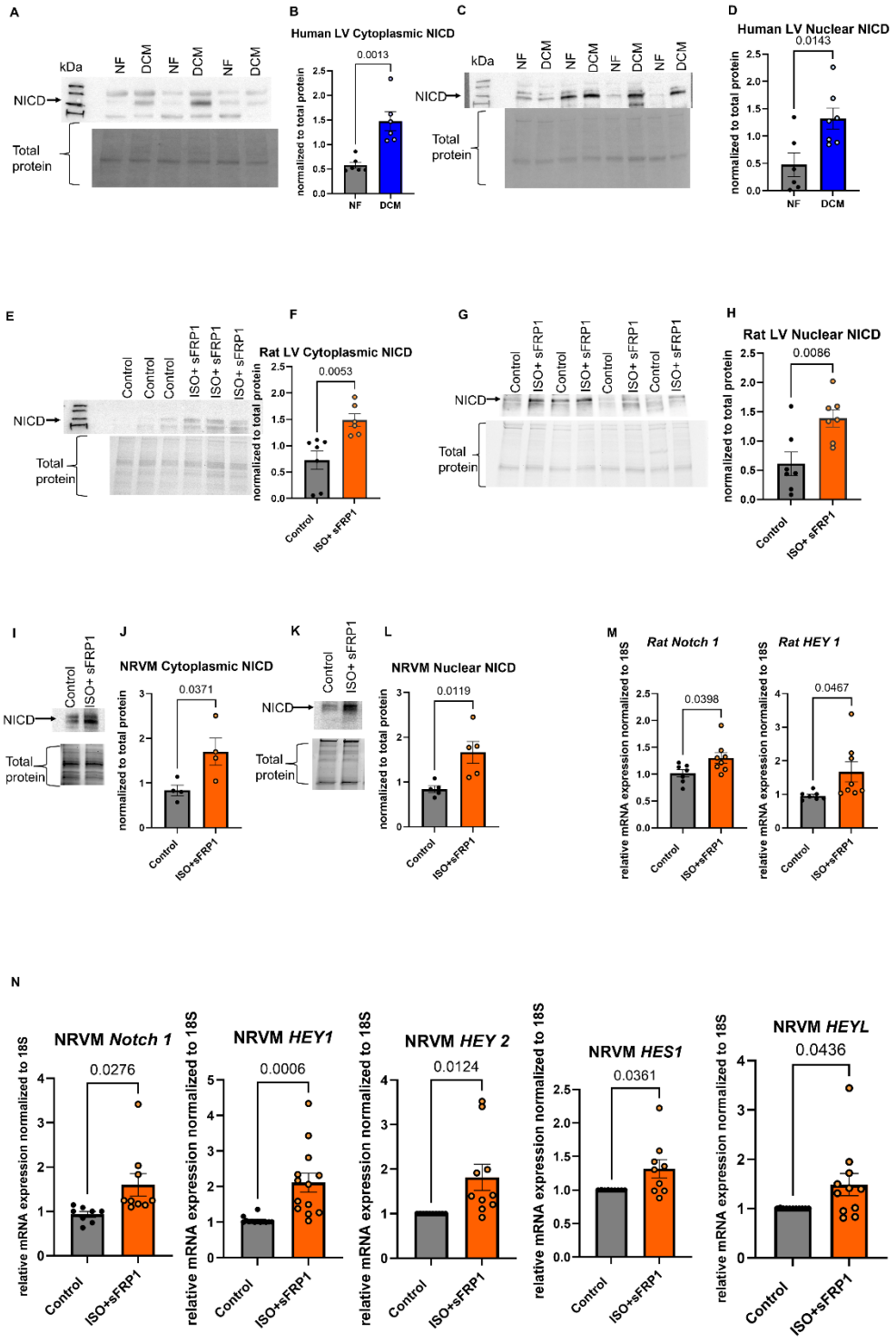
A
kDa
NF
DCM
NF
DCM
NF
DCM
NICD
Total protein
B
Human LV Cytoplasmic NICD
0.0013
normalized to total protein
NF
DCM
C
kDa
NF
DCM
NF
DCM
NF
DCM
NICD
Total protein
D
Human LV Nuclear NICD
0.0143
normalized to total protein
NF
DCM
E
Control
Control
Control
ISO+ sFRP1
ISO+ sFRP1
ISO+ sFRP1
NICD
Total protein
F
Rat LV Cytoplasmic NICD
0.0053
normalized to total protein
Control
ISO+ sFRP1
G
Control
ISO+ sFRP1
Control
ISO+ sFRP1
Control
ISO+ sFRP1
Control
ISO+ sFRP1
NICD
Total protein
H
Rat LV Nuclear NICD
0.0086
normalized to total protein
Control
ISO+ sFRP1
I
Control
ISO+ sFRP1
NICD
Total protein
J
NRVM Cytoplasmic NICD
0.0371
normalized to total protein
Control
ISO+sFRP1
K
Control
ISO+ sFRP1
NICD
Total protein
L
NRVM Nuclear NICD
0.0119
normalized to total protein
Control
ISO+sFRP1
M
Rat Notch 1
0.0398
relative mRNA expression normalized to 18S
Control
ISO+sFRP1
Rat HEY 1
0.0467
relative mRNA expression normalized to 18S
Control
ISO+sFRP1
N
NRVM Notch 1
0.0276
relative mRNA expression normalized to 18S
Control
ISO+sFRP1
NRVM HEY1
0.0006
relative mRNA expression normalized to 18S
Control
ISO+sFRP1
NRVM HEY 2
0.0124
relative mRNA expression normalized to 18S
Control
ISO+sFRP1
NRVM HES1
0.0361
relative mRNA expression normalized to 18S
Control
ISO+sFRP1
NRVM HEYL
0.0436
relative mRNA expression normalized to 18S
Control
ISO+sFRP1

876

877 Figure 5. Levels of NICD are increased in nuclear and cytoplasmic fractions in *vivo*, *in*
878 *vitro* and in explanted human DCM hearts.

879 (A-D) Western blot showing increased protein levels of NICD in the cytoplasm (A)
880 and nuclear fractions (C) of NF vs DCM human LV tissue. (B) and (D) represent
881 quantification of (A) and (C) respectively. Cytoplasmic n=6/group, Nuclear
882 n=7/group.

883 (E-H) Western blot showing increased protein levels of NICD in the cytoplasm (E)
884 and nuclear fractions (G) of ISO+sFRP1 vs vehicle-treated control rat LV tissue.
885 (F) and (H) represent the quantification of (E) and (G) respectively. Cytoplasmic
886 n=6/group, Nuclear n=7/group.

887 (I-L) Western blot showing the increased protein levels of NICD in the cytoplasm (I)
888 and nuclear fractions (K) of ISO+sFRP1 vs vehicle-treated NRVMs. (J) and (L)
889 represent the quantification of (I) and (K) respectively. Cytoplasmic n = 4
890 independent NRVM preps, nuclear n = 5 independent NRVM preps. NICD. Notch
891 Intracellular domain, NRVMs, neonatal rat ventricular myocytes.

892 (M) RT-qPCR of Notch1 and Hey1 gene expression in ISO+sFRP1 rat LV tissue
893 compared to Control. Gene expression was normalized to 18S, and data are
894 presented as a relative fold change to Controls. n=8/group.

895 (N) RT-qPCR of Notch target genes in NRVMs treated with vehicle (Control) and
896 ISO+sFRP1. Expression of Notch1, Hey1, HEY2, HES1 and HEYL genes. Gene
897 expression was normalized to 18S, and data are presented as a relative fold
898 change to Controls. n = 6 independent NRVM preps/group. NF, non-failing; DCM,

899 dilated cardiomyopathy; NICD, Notch Intracellular domain. Unpaired 2-tailed t

900 test was used in analysis. P-values are notated in each graph.

901
902

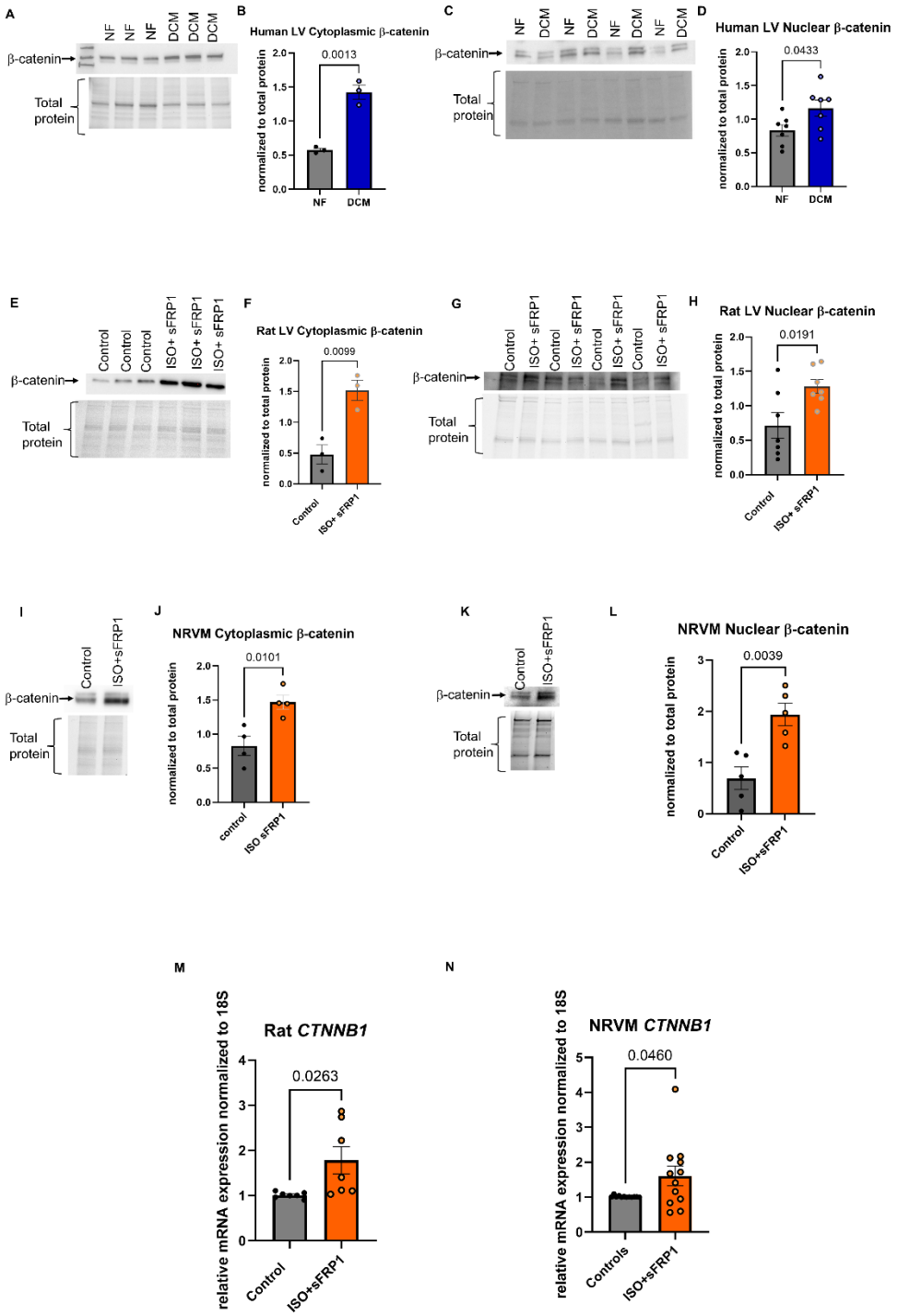
A
NF
NF
NF
DCM
DCM
DCM
β-catenin
Total protein
B
Human LV Cytoplasmic β-catenin
0.0013
normalized to total protein
NF
DCM
C
NF
DCM
NF
DCM
NF
DCM
β-catenin
Total protein
D
Human LV Nuclear β-catenin
0.0433
normalized to total protein
NF
DCM
E
Control
Control
Control
ISO+ sFRP1
ISO+ sFRP1
ISO+ sFRP1
β-catenin
Total protein
F
Rat LV Cytoplasmic β-catenin
0.0099
normalized to total protein
Control
ISO+ sFRP1
G
Control
ISO+ sFRP1
Control
ISO+ sFRP1
Control
ISO+ sFRP1
β-catenin
Total protein
H
Rat LV Nuclear β-catenin
0.0191
normalized to total protein
Control
ISO+ sFRP1
I
Control
ISO+sFRP1
β-catenin
Total protein
J
NRVM Cytoplasmic β-catenin
0.0101
normalized to total protein
control
ISO sFRP1
K
Control
ISO+sFRP1
β-catenin
Total protein
L
NRVM Nuclear β-catenin
0.0039
normalized to total protein
Control
ISO+sFRP1
M
Rat CTNNB1
0.0263
relative mRNA expression normalized to 18S
Control
ISO+sFRP1
N
NRVM CTNNB1
0.0460
relative mRNA expression normalized to 18S
Controls
ISO+sFRP1

903

904 Figure 6. Levels of β-catenin are increased in nuclear and cytoplasmic fractions *in vivo*,
905 *in vitro* and in explanted human DCM hearts.

906 (A-D) Western blot showing increased protein levels of β-catenin in the cytoplasm
907 (A) and nuclear fractions (C) of NF and DCM explanted human LV tissue. (B) and
908 (D) represent the quantification of (A) and (C) respectively. NF, non-failing; DCM,
909 dilated cardiomyopathy; cytoplasmic n=3/group, nuclear n=7/group.

910 (E-H) Western blot showing increased protein levels of β-catenin in the cytoplasm
911 (E) and nuclear fractions (G) of ISO+sFRP1 vs vehicle-treated control rat LV
912 tissue. (F) and (H) represent the quantification of (E) and (G) respectively.
913 Cytoplasmic n=3/group, nuclear, n=7/group.

914 (I-L) Western blot showing increased protein levels of β-catenin in the cytoplasm (I)
915 and nuclear fractions (K) of ISO+sFRP1 vs vehicle-treated NRVMs. (J) and (L)
916 represent the quantification of (I) and (K) respectively. Cytoplasmic and nuclear
917 fractions from n=4 independent NRVM preps.

918 (M) RT-qPCR of CTNNB1 gene expression in ISO+sFRP1-treated rat LV tissue
919 compared to Control. Gene expression was normalized to 18S, and data are
920 presented as a relative fold change to Controls. n=7/group

921 (N) RT-qPCR of CTNNB1 gene expression in NRVMs treated with vehicle (Control)
922 or ISO+sFRP1. Gene expression was normalized to 18S, and data are presented
923 as a relative fold change to Controls. n=8 independent NRVM preps/group

924 NRVMs, neonatal rat ventricular myocytes. Unpaired 2-tailed t test was used in
925 analysis. p-values are notated in each graph.

926

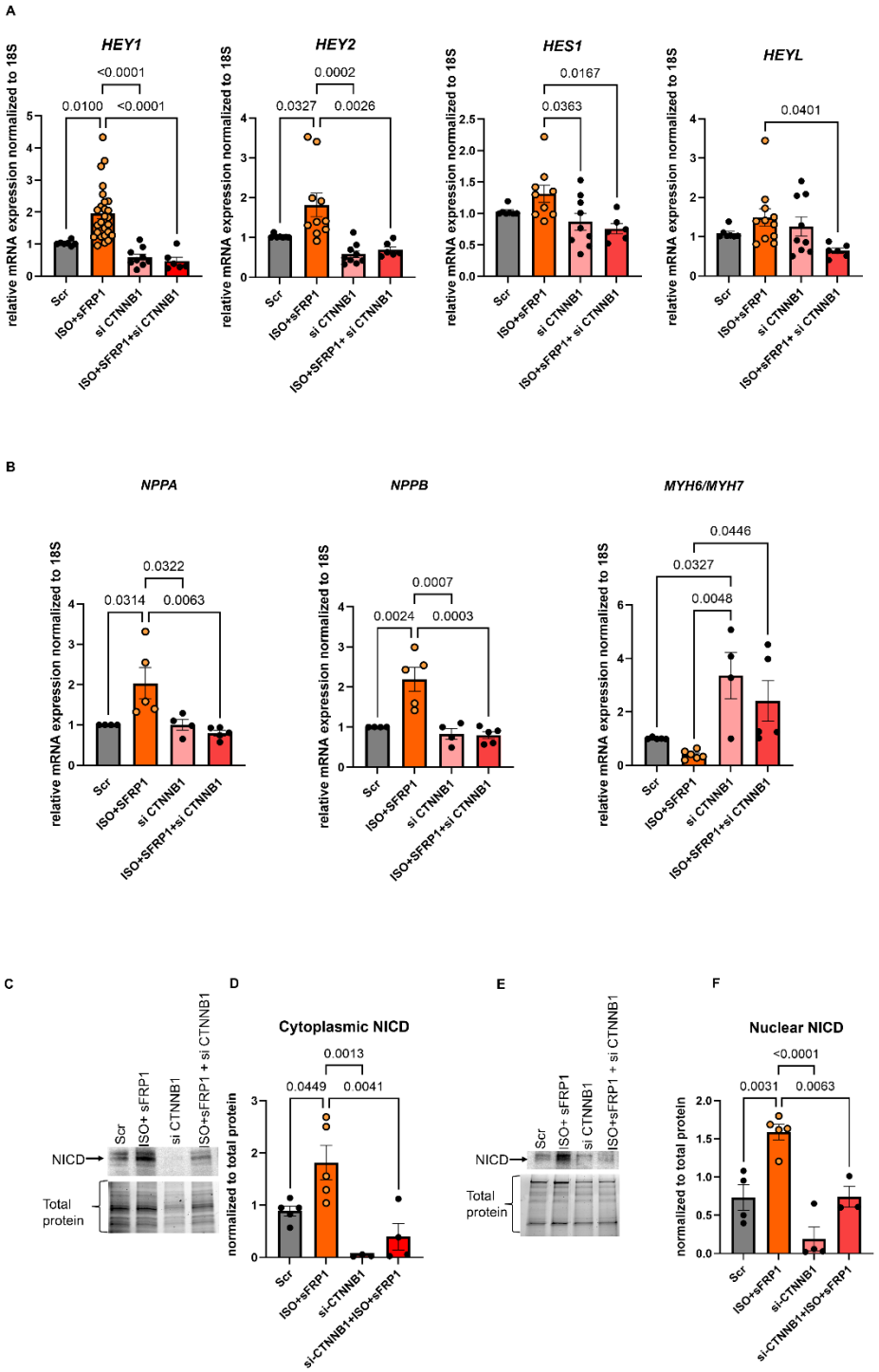
A
HEY1
HEY2
HES1
HEYL
relative mRNA expression normalized to 18S
<0.0001
0.0100
<0.0001
0.0002
0.0327
0.0026
0.0167
0.0363
0.0401
Scr
ISO+sFRP1
si CTNNB1
ISO+SFRP1+si CTNNB1
B
NPPA
NPPB
MYH6/MYH7
0.0322
0.0314
0.0063
0.0007
0.0024
0.0003
0.0446
0.0327
0.0048
C
NICD
Total protein
Scr
ISO+ sFRP1
si CTNNB1
ISO+sFRP1 + si CTNNB1
D
Cytoplasmic NICD
normalized to total protein
0.0013
0.0449
0.0041
si-CTNNB1+ISO+sFRP1
E
F
Nuclear NICD
<0.0001
0.0031
0.0063

927

928 Figure 7. β-catenin contributes to Notch activation, and inhibiting β-catenin prevents
929 pathological remodeling in ISO+sFRP1-treated cells.
930 (A) RT-qPCR of Notch target gene expression in NRVMs transfected with scrambled
931 control siRNA (scr) or siCTNNB1, and treated with vehicle (Control) or ISO+sFRP1.
932 Expression of *Hey1, HEY2, HES1* and *HEYL* genes. Gene expression was
933 normalized to 18S, and data are presented as a relative fold change to Controls.
934 *n*=6 independent NRVM preps/group
935 (B) RT-qPCR of FGP gene expression in NRVMs transfected with scrambled control
936 siRNA (scr) or siCTNNB1 and treated with vehicle (Control) or ISO+sFRP1.
937 Expression of *NPPA, NPPB,* and ratio of *MYH6* to *MYH7*. Gene expression was
938 normalized to 18S, and data are presented as a relative fold change to Controls.
939 n=4 independent NRVM preps/group
940 (C-F) Western blot showing reduced protein levels of NICD in the cytoplasm and
941 nuclear fractions (E) of NRVMs treated with ISO+sFRP1 and transfected with si-
942 CTNNB1 when compared to ISO+sFRP1-treated cells. (D) and (F) represent the
943 quantification of (C) and (E) respectively. n=3 independent NRVM preps/group. NICD,
944 Notch Intracellular domain, NRVMs, neonatal rat ventricular myocytes
945

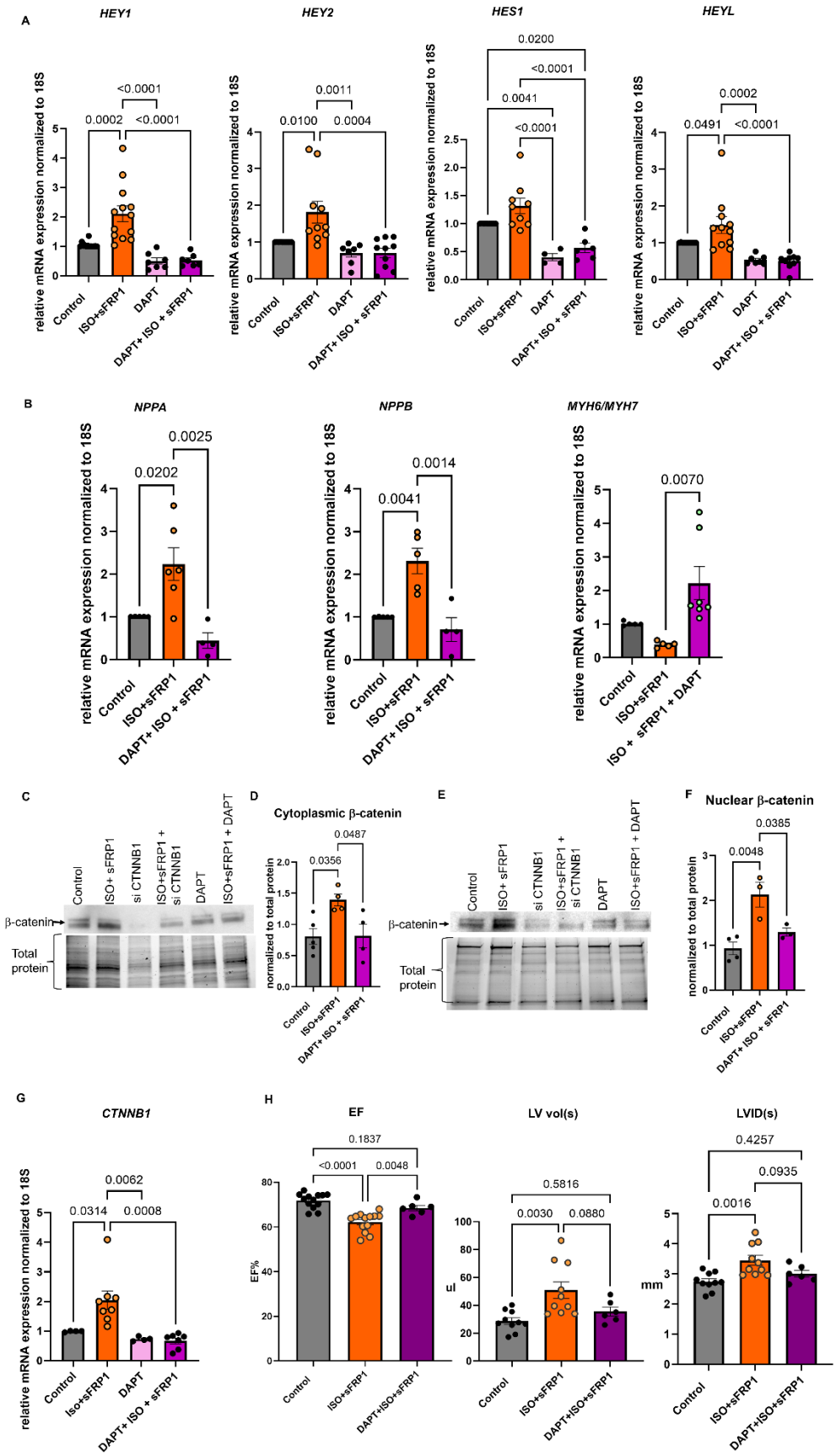
A
HEY1
HEY2
HES1
HEYL
relative mRNA expression normalized to 18S
Control
ISO+sFRP1
DAPT
DAPT+ ISO + sFRP1
B
NPPA
NPPB
MYH6/MYH7
ISO + sFRP1 + DAPT
C
Control
ISO+ sFRP1
si CTNNB1
ISO+sFRP1 + si CTNNB1
DAPT
ISO+sFRP1 + DAPT
β-catenin
Total protein
D
Cytoplasmic β-catenin
normalized to total protein
E
F
Nuclear β-catenin
G
CTNNB1
H
EF
LV vol(s)
LVID(s)
EF%
ul
mm
DAPT+ISO+sFRP1

946

947 Figure 8. Notch contributes to β-catenin activation, and inhibiting Notch prevents
948 pathological remodeling and cardiac dysfunction.
949 (A) RT-qPCR of Notch target gene expression (*HEY1, HEY2, HES1* and *HEYL)* in
950 NRVMs treated with vehicle (Control), ISO+sFRP1, DAPT (20μM) or
951 ISO+sFRP1+DAPT. Gene expression was normalized to 18S, and data are
952 presented as a relative fold change to Controls. *n* = 7 independent NRVM
953 preps/group
954 (B) RT-qPCR of FGP in NRVMs treated with vehicle (Control), ISO+sFRP1, DAPT
955 (20μM) or ISO+sFRP1+DAPT. Gene expression was normalized to 18S, and data
956 are presented as a relative fold change to Controls. *n* = 5 independent NRVM
957 preps/group
958 (C) Western blot showing the reduced protein levels of β-catenin in the cytoplasm and
959 nuclear fractions (E) of ISO+sFRP1+DAPT or ISO+sFRP1-treated NRVMs. (D) and
960 (F) represent the quantification of (C) and (E) respectively. *P*-values are notated in
961 each graph. *n* = 4 independent NRVM preps/group. NRVM, neonatal rat ventricular
962 myocytes
963 (G) RT-qPCR of CTNNB1 gene expression in NRVMs treated with vehicle (Control),
964 ISO+sFRP1, DAPT (20μM) and ISO+Sfrp1+DAPT. Gene expression was
965 normalized to 18S, and data are presented as a relative fold change to Controls.
966 Tukey's multiple comparisons test was used for all data sets. Control, n = 4,
967 ISO+sFRP1 n = 8, DAPT n = 4 and ISO+sFRP1+DAPT n = 7
968 (H) EF, LV vol(s) and LVID(s) of neonatal rats treated with Control, ISO+sFRP1 and
969 DAPT ISO+sFRP1. Control n=13, ISO+sFRP1 n=13. DAPT+ISO+sFRP1 n=6.

970 EF: ejection fraction; LV vol(s), Left ventricular volume in systole; LVID. Left
971 ventricular internal diameter in systole. Tukey's multiple comparisons test was
972 used for all data sets. P-values are notated in the graph.
973